



LIBRARY
OF THE
UNIVERSITY
OF ILLINOIS

621.365

Il 655te

no. 40-49

cap. 2



Digitized by the Internet Archive
in 2013

<http://archive.org/details/radiationpattern41balm>

ANTENNA LABORATORY

Technical Report No. 41

THE RADIATION PATTERN OF A DIPOLE
ON A FINITE DIELECTRIC SHEET

by

Keith G. Balmain

1 August 1959

Contract AF33(616)-6079

Project No. 9-(13-6278) Task 40572

Sponsored by:

WRIGHT AIR DEVELOPMENT CENTER

Electrical Engineering Research Laboratory
Engineering Experiment Station
University of Illinois
Urbana, Illinois

621.305

IL655te

no. 41

cop. 2

ABSTRACT

When a metallic antenna is "printed" on the surface of a dielectric sheet, the original radiation pattern is altered by the presence of the dielectric. This report considers the case of a half-wave dipole antenna mounted on the surface of a thin, rectangular dielectric sheet. For this case, the pattern changes due to the dielectric are found to be quite large, even for very thin sheets. Theoretical radiation pattern calculations are presented and they agree with the experimental patterns for thin sheets. The results obtained provide a basis for estimating the radiation pattern perturbations due to the dielectric for a fairly wide range of dielectric constant and sheet dimensions.

ACKNOWLEDGMENT

The author is very grateful for the helpful advice from Dr. P. E. Mayes who suggested the problem, and from Dr. G. A. Deschamps who recommended the Fresnel integral analysis. He also wishes to acknowledge the many discussions with Dr. Y. T. Lo, Dr. W. L. Weeks and the other members of the Antenna Laboratory staff.

The author appreciates the assistance of T. M. Lahey and M. L. Harding who carried out the computer programming, and J. Fisk, D. Butcher and J. Flaherty who made the experimental measurements.

CONTENTS

1. Introduction	1
2. Experiments	7
3. Theory	19
The Iteration Series Solution	21
The Fresnel Integral Solution	23
Asymptotic Behavior of the Fresnel Integral Solution	26
4. Comments	29
5. Conclusions	32
6. Bibliography	33
Appendix A	34
Appendix B	43
Appendix C	50
Appendix D	58
Appendix E	62

ILLUSTRATIONS

Figure
Number

1.	Dipole "Printed" on a Dielectric Sheet	2
2.	The Experimental Model	2
3.	The Ground-Plane Version of the Experimental Model	2
4.	The Theoretical Model	4
5.	The Hankel Function Large-Argument Approximation	4
6.	Radiation Patterns: $\ell = .5\lambda$, $\epsilon_r = 2.55$	9
7.	Radiation Patterns: $\ell = 1.0\lambda$, $\epsilon_r = 2.55$	10
8.	Radiation Patterns: $\ell = 1.5\lambda$, $\epsilon_r = 2.55$	11
9.	Radiation Patterns: $\ell = 2.0\lambda$, $\epsilon_r = 2.55$	12
10.	Radiation Patterns: $\ell = 2.5\lambda$, $\epsilon_r = 2.55$	13
11.	Radiation Patterns: $\ell = 3.0\lambda$, $\epsilon_r = 2.55$	14
12.	Graph of Maximum Radiation Pattern Error $\ell = .5\lambda$	16
13.	Graph of Maximum Radiation Pattern Error $\ell = 1.0\lambda$	16
14.	Graph of Maximum Radiation Pattern Error $\ell = 1.5\lambda$	17
15.	Graph of Maximum Radiation Pattern Error $\ell = 2.0\lambda$	17
16.	Graph of Maximum Radiation Pattern Error $\ell = 2.5\lambda$	18
17.	Graph of Maximum Radiation Pattern Error $\ell = 3.0\lambda$	18
18.	Comparison of the Iteration Series, Fresnel Integral and "Two-Source Equivalent" Radiation Patterns	25

1. INTRODUCTION

The University of Illinois Antenna Laboratory some time ago set up a facility for etching "printed circuit" antennas on copper-clad dielectric sheets. Accordingly, it was decided to investigate the effects of a finite dielectric sheet when used as the base for a printed antenna. This report is concerned with one aspect of the problem--that of determining the radiation pattern of a half-wave dipole antenna which is on the surface of a thin, rectangular dielectric sheet and located midway between the edges as shown in Figure 1.

In order to make the experimental model more suitable for theoretical study, it was decided to perform the experiments with the dipole embedded inside the dielectric sheet, midway between its two faces as in Figure 2. This approach was chosen after experiments showed that, for thin sheets, there is negligible difference between patterns taken with the dipole inside the dielectric and those taken with the dipole on its surface. A further simplification resulted from an application of the theory of images which permits a conducting plane to be passed through the center of the dipole and perpendicular to it. This made it possible for the radiation pattern measurements to be carried out on a ground plane as shown in Figure 3.

So far, we have decided on an antenna model suitable for experimental purposes. However, some further simplifications must be made if we are to have an antenna model suitable for theoretical calculations. Since experiments showed that the pattern perturbations in the (x, y) plane were much greater than those in the other two principal planes, it was

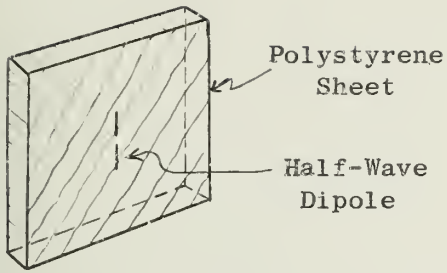


FIGURE 1
Dipole "Printed"
on a
Dielectric Sheet

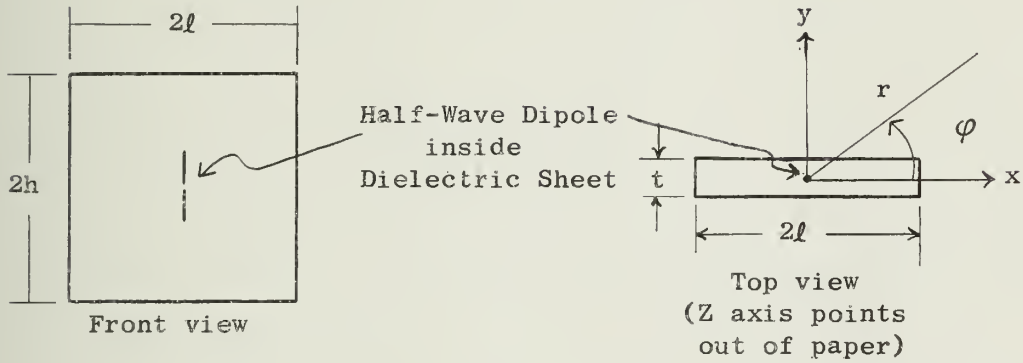


FIGURE 2
The Experimental Model

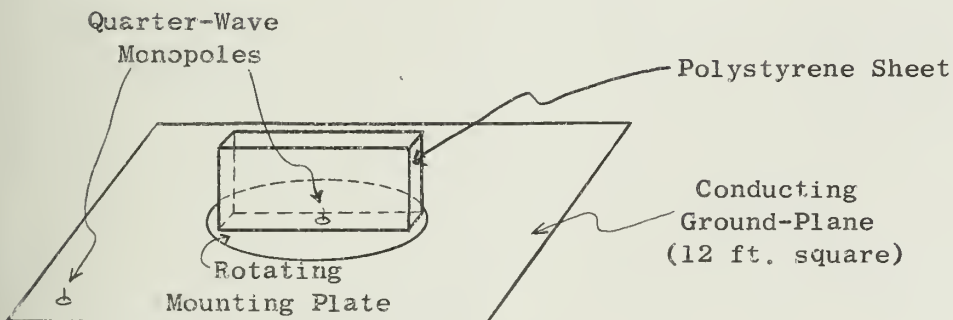


FIGURE 3
The Ground-Plane Version of the Experimental Model

decided to consider only the (x, y) plane pattern in this report. This not only simplifies the experimental work but also suggests reduction of the three-dimensional theoretical problem to a two-dimensional one. This can be done by considering an equivalent mathematical model having an infinite line source embedded in an infinite dielectric strip as shown in Figure 4. Assuming the applicability of this mathematical model implies that the dimension h (of the experimental model) must be great enough so that changing it appreciably has no effect on the (x, y) plane pattern (see discussion in Chapter 2). Using the theoretical model described, it is possible to derive an integral equation for the electric field at any point in space. In this equation, the integration is over the cross-sectional area of the dielectric strip. However, the number of variables of integration can be reduced from two to one by assuming that the dielectric sheet is very thin and that there is no field variation across its narrow dimension.

The radiation field was calculated by using the assumption that the field in the dielectric sheet is the same as the incident field in free space. Such an approximation permitted the integration to be carried out numerically on a digital computer. This approach is equivalent to using the first term in the iteration series solution for the field inside the sheet. Therefore this solution will be referred to as the "iteration series" solution. It is discussed further in Chapter 3 and Appendix A.

A consideration of the radiation patterns presented in Chapter 2 shows that even very thin dielectric sheets (about a hundredth of a wavelength thick) can have a marked effect on the dipole pattern. Fortunately

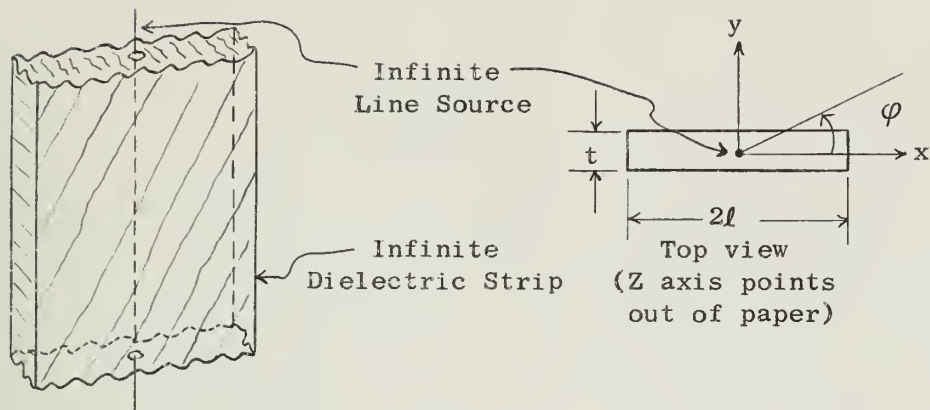


FIGURE 4

THE THEORETICAL MODEL

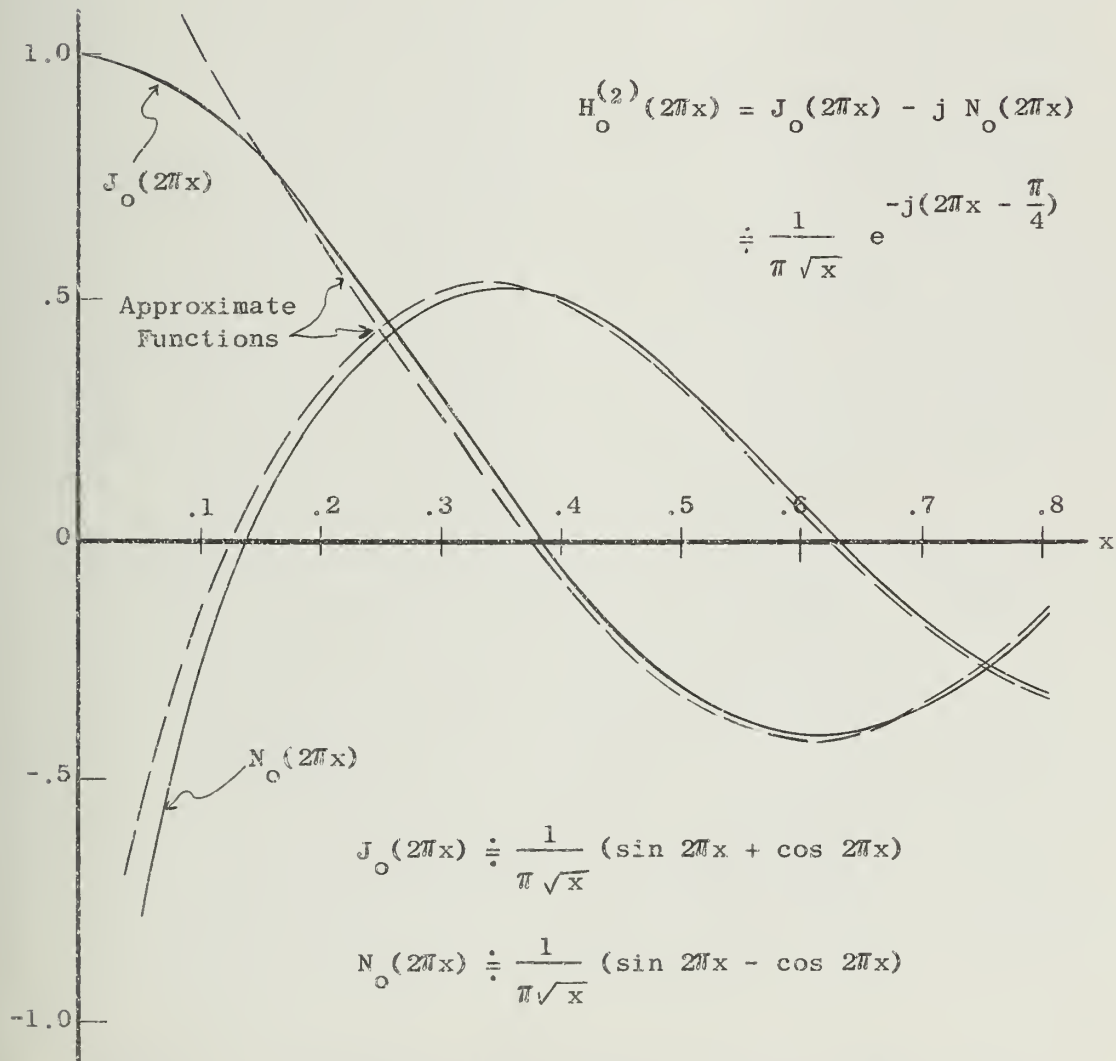


FIGURE 5. THE HANKEL FUNCTION LARGE-ARGUMENT APPROXIMATION

this effect is predictable when the dielectric is thin as the theoretical results show. At this point some comment on the word "thin" seems to be appropriate; a "thin" polystyrene sheet will be understood to mean a sheet less than three hundredths of a wavelength thick. As might be expected, the usefulness of the theory is limited not only by the sheet thickness but also by its dielectric constant. Relative dielectric constants above four or five severely restrict the applicability of the theoretical approach described in this report.

The experimental results shown are for polystyrene with a dielectric constant of 2.55 and most of the measurements were carried out at 5000 mc. However, the graphs shown can be extended to other parameter values by use of the fact that for constant sheet length $\frac{l}{\lambda}$ and constant angle φ , the pattern perturbation magnitude is a function of the factor $(\epsilon_r - 1) \frac{t}{\lambda}$ where $\frac{t}{\lambda}$ is the sheet thickness in wavelengths and ϵ_r is the relative dielectric constant. This means that, for a fixed frequency, the same radiation pattern will apply to the two cases $\epsilon_r = 2.5$, $t = .02\lambda$ and $\epsilon_r = 4.0$, $t = .01\lambda$. The theory breaks down for thick sheets but the experimental results indicate the pattern shapes to be expected.

Another approach to the solution of the integral equation is helpful in interpreting the phenomena observed. The so-called "iteration-series" approach already mentioned requires the numerical evaluation of an integral over the range $(-l, l)$. If the integration over this range is broken up into integrations over the ranges $(-\infty, -l)$, (l, ∞) and $(-\infty, \infty)$, and if the Hankel function $H_0^{(2)}(2\pi \frac{l}{\lambda})$ can be represented by its "large-argument" approximation for fairly small values of $\frac{l}{\lambda}$, then the radiation

pattern can be expressed in terms of Fresnel integrals. One of the advantages of this "Fresnel integral" solution is that the integrals have asymptotic expansions valid for values of φ not too close to 0° or 180° . For very thin dielectric the asymptotic formulae show that a dielectric strip can be represented approximately by two line sources in free space in positions corresponding to the strip edges (at $x = \pm \ell$). This will be referred to as the "two-source equivalent".

As mentioned above, the accuracy of the Fresnel integral solution depends on how closely the Hankel function $H_0^{(2)}(2\pi x)$ is approximated by its large-argument asymptotic form. The Hankel function and its approximation are compared in Figure 5 and the approximate formula error is less than .015 for $x \geq .5$. Thus the Fresnel integral solution and the interaction series solution should differ by a negligible amount as long as the dimension ℓ is at least a half wavelength.

2. EXPERIMENTS

For convenience in making the measurements, the experiments were set up on a ground plane as shown in Figure 3 and the field measurements were made by using the corner monopole for transmitting and the center monopole for receiving. A bolometer was used as the detecting element and most of the measurements were carried out at 5000 mc. All the radiation patterns show relative values of the electric field intensity E .

Experimentally it was found that the slab height (h) had negligible effect on the radiation pattern, provided that the height was greater than about three wavelengths. Accordingly a height of four wavelengths was chosen for the experiments performed. The fact that the antenna pattern is independent of h (for h sufficiently large) is a partial justification for the use of a mathematical model with h equal to infinity. Probably the radiation pattern is independent of h because (in free space at least) the monopole radiates no energy in the z -direction. This means that the top edge of the dielectric slab would intercept a relatively small portion of the total radiated energy if h were large.

The theory indicates that the pattern perturbations depend on $(\epsilon_r - 1) \frac{t}{\lambda}$. Experimentally this result was verified by selecting various combinations of frequency, sheet thickness and dielectric constant to give the same value of $(\epsilon_r - 1) \frac{t}{\lambda}$ while the sheet length $\frac{l}{\lambda}$ was held constant. The patterns obtained are not shown in this report but they were essentially identical for thin sheets ($t < .03\lambda$) and roughly similar even for the thickest sheets considered.

The radiation patterns exhibit some interesting characteristics, the most prominent of which is the "end fire" lobe at $\varphi = 0^\circ$ (see Figures 6 to 11). It is always present and becomes narrower as the length $\frac{\ell}{\lambda}$ is increased. In addition to the major lobe some side lobes appear, their number and position depending on $\frac{\ell}{\lambda}$. Let us denote a free space wavelength by λ and the wavelength of the lowest order TE mode propagated along an infinite dielectric sheet by λ_g . It will be assumed that λ_g is approximately the wavelength of waves propagating along a finite dielectric sheet and generated by a line source as in the practical problem considered. For the case of thin sheets $\lambda_g \doteq \lambda$ (see Appendix E) and the radiation patterns indicate that the number of minima in a 180° sector ($0^\circ \leq \varphi \leq 180^\circ$) increases by one for every $\frac{\lambda}{2}$ increase in ℓ . This rule breaks down for the thicker sheets for which $\lambda_g \neq \lambda$ (see Figures 10 and 11 for the $\frac{1}{8}$ " and $\frac{1}{4}$ " sheets) but the rule seems to hold for all thicknesses considered if we write λ_g in place of λ . Thus the rule is that the number of nulls in the range $0^\circ \leq \varphi \leq 180^\circ$ increases by one for every $\frac{\lambda_g}{2}$ increase in the length ℓ . Values of $\frac{\lambda_g}{\lambda}$ for various sheet thicknesses are tabulated in Appendix E where it can be seen that $\frac{\lambda_g}{\lambda}$ is always somewhat less than λ . Since the values of $\frac{\lambda_g}{\lambda}$ decrease rapidly for $t > .05292\lambda$ ($\frac{1}{8}$ ") it is not surprising that the effects of low propagation velocity show up in the radiation patterns only for $t = .1058\lambda$ ($\frac{1}{4}$ ").

Another interesting aspect of the radiation patterns is the null depth, a quantity which increases sharply as the slab thickness and/or dielectric constant increases. In all cases the null beside the major lobe (which we shall call the principal null) is the deepest while all the

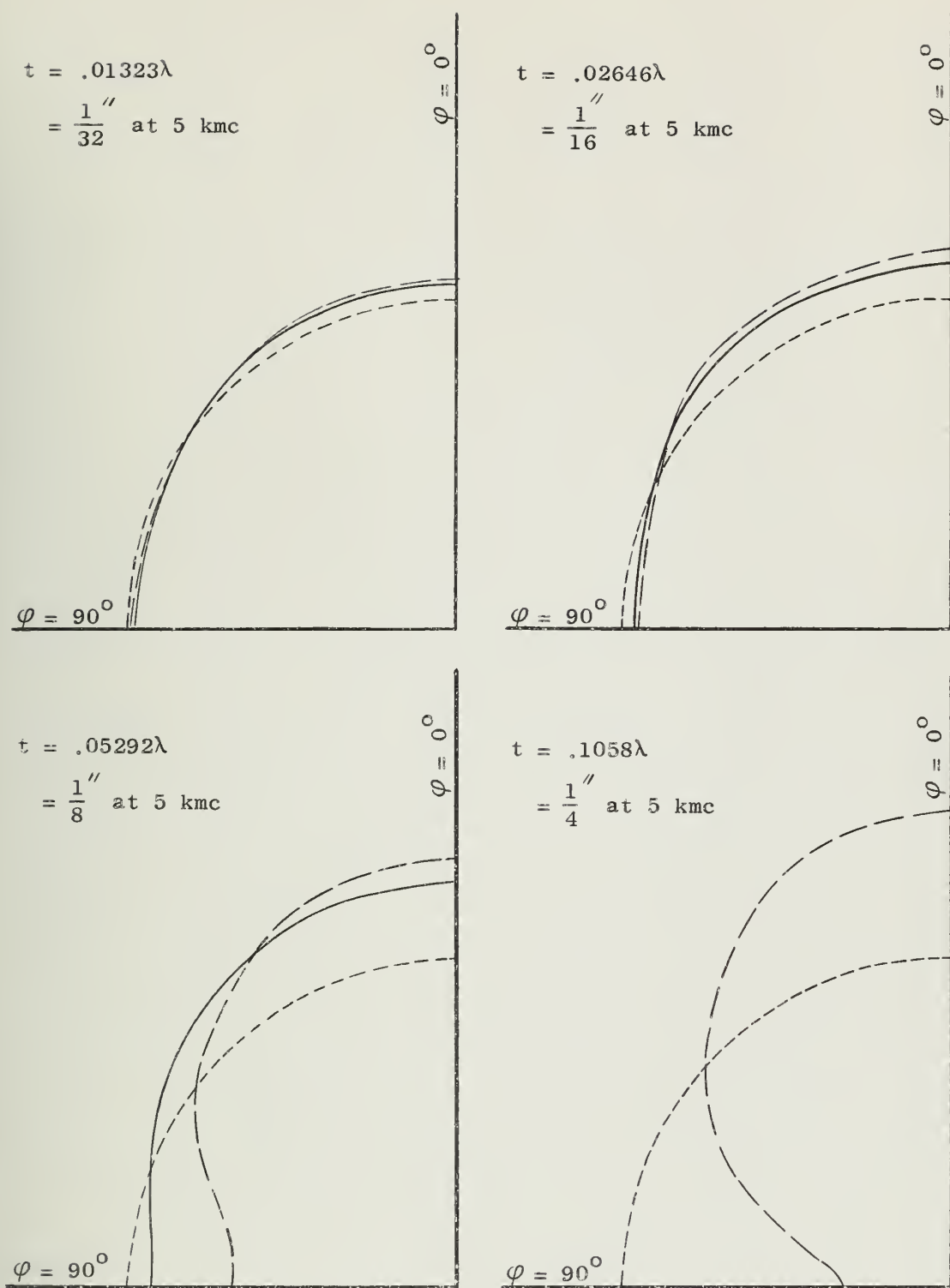


FIGURE 6. RADIATION PATTERNS: $l = .5\lambda$, $\epsilon_r = 2.55$

- — — — — Experimental Pattern
- — — — — Theoretical Pattern (Iteration Series)
- - - - - Unperturbed Dipole Pattern (Circle)

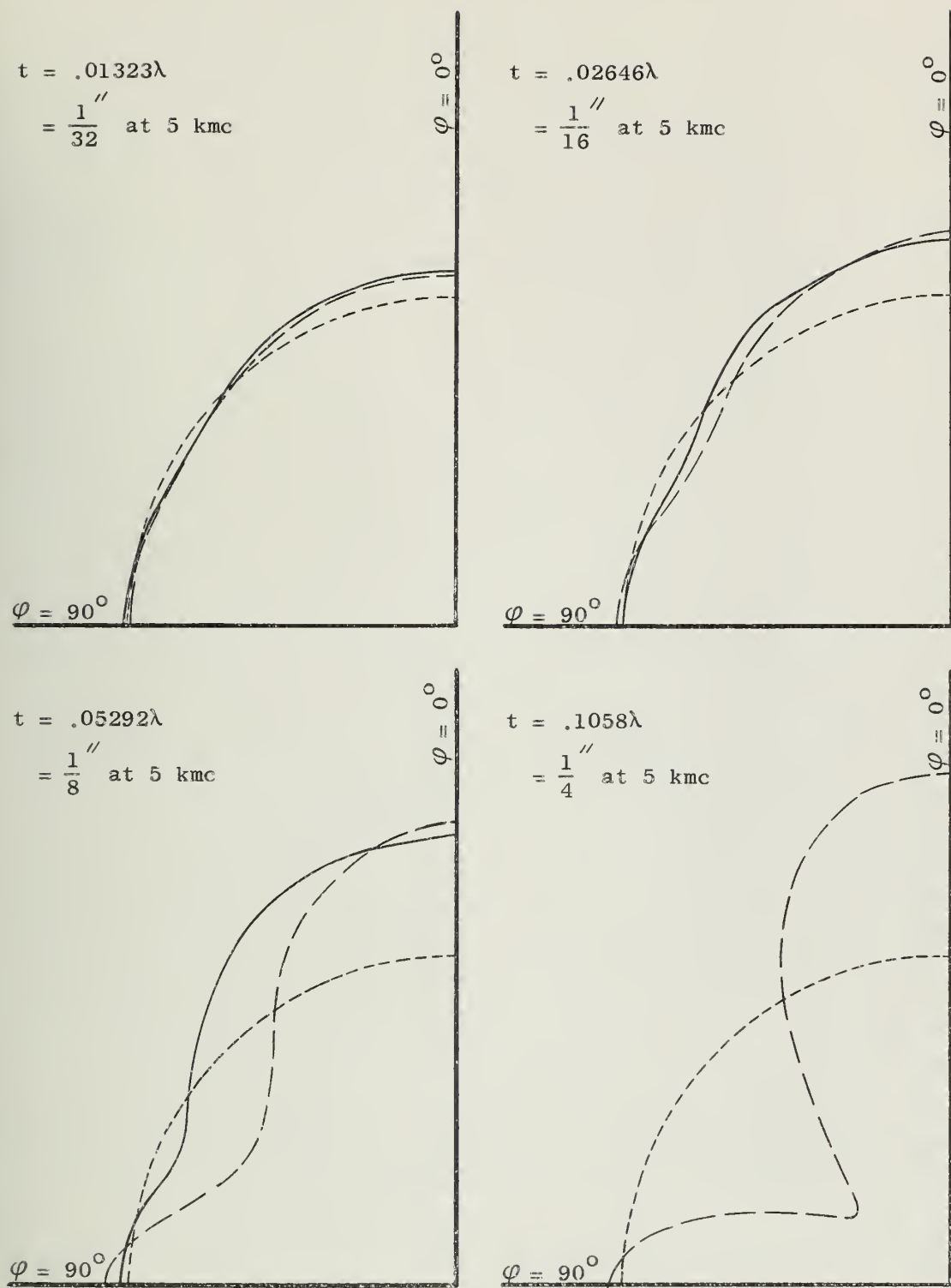


FIGURE 7. RADIATION PATTERNS: $l = 1.0\lambda$, $\epsilon_r = 2.55$

- Experimental Pattern
- Theoretical Pattern (Iteration Series)
- Unperturbed Dipole Pattern (Circle)

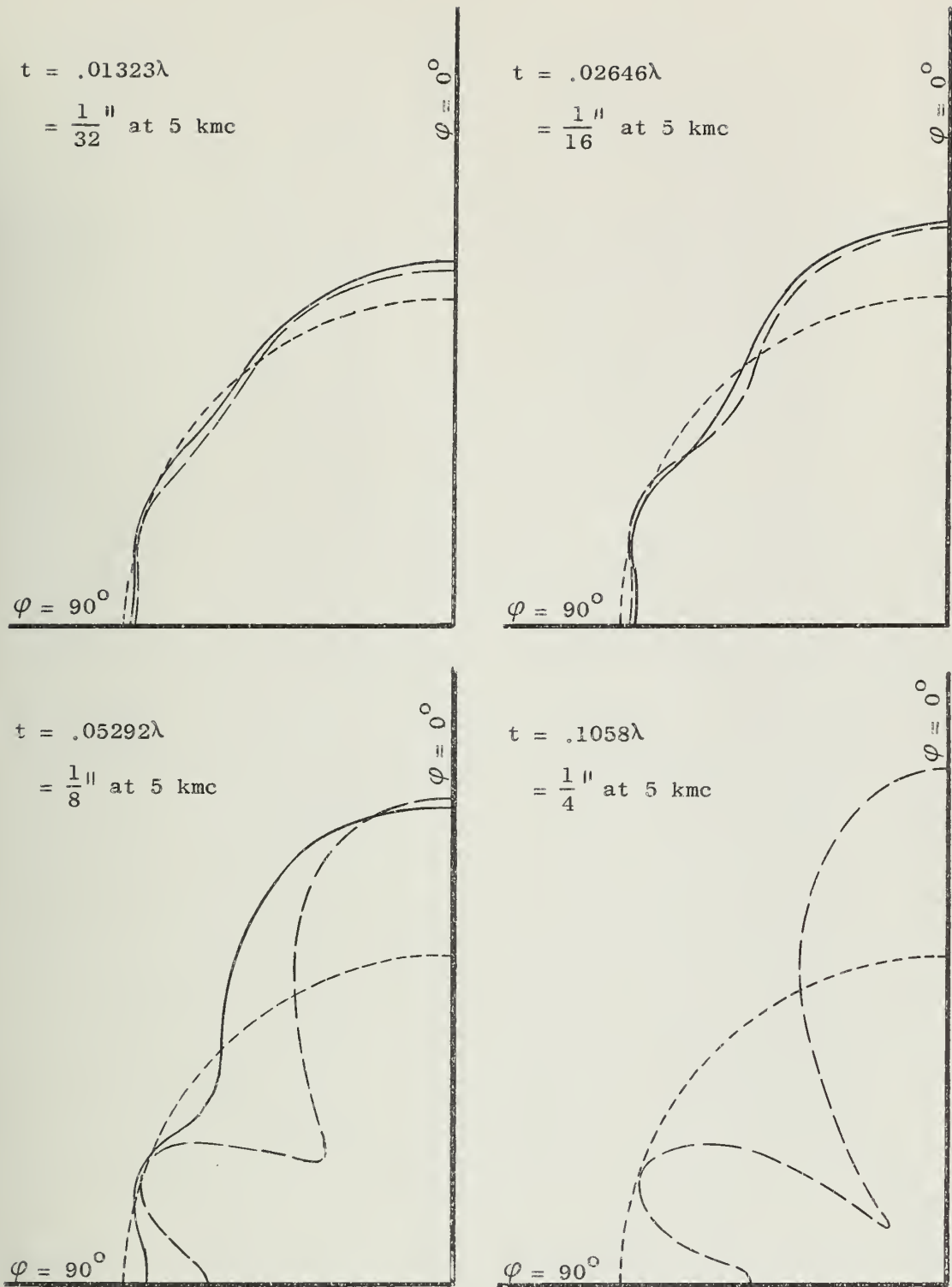


FIGURE 8. RADIATION PATTERNS: $l = 1.5\lambda$, $\epsilon_r = 2.55$

- — — — — Experimental Pattern
 ————— Theoretical Pattern (Iteration Series)
 - - - - - Unperturbed Dipole Pattern (Circle)

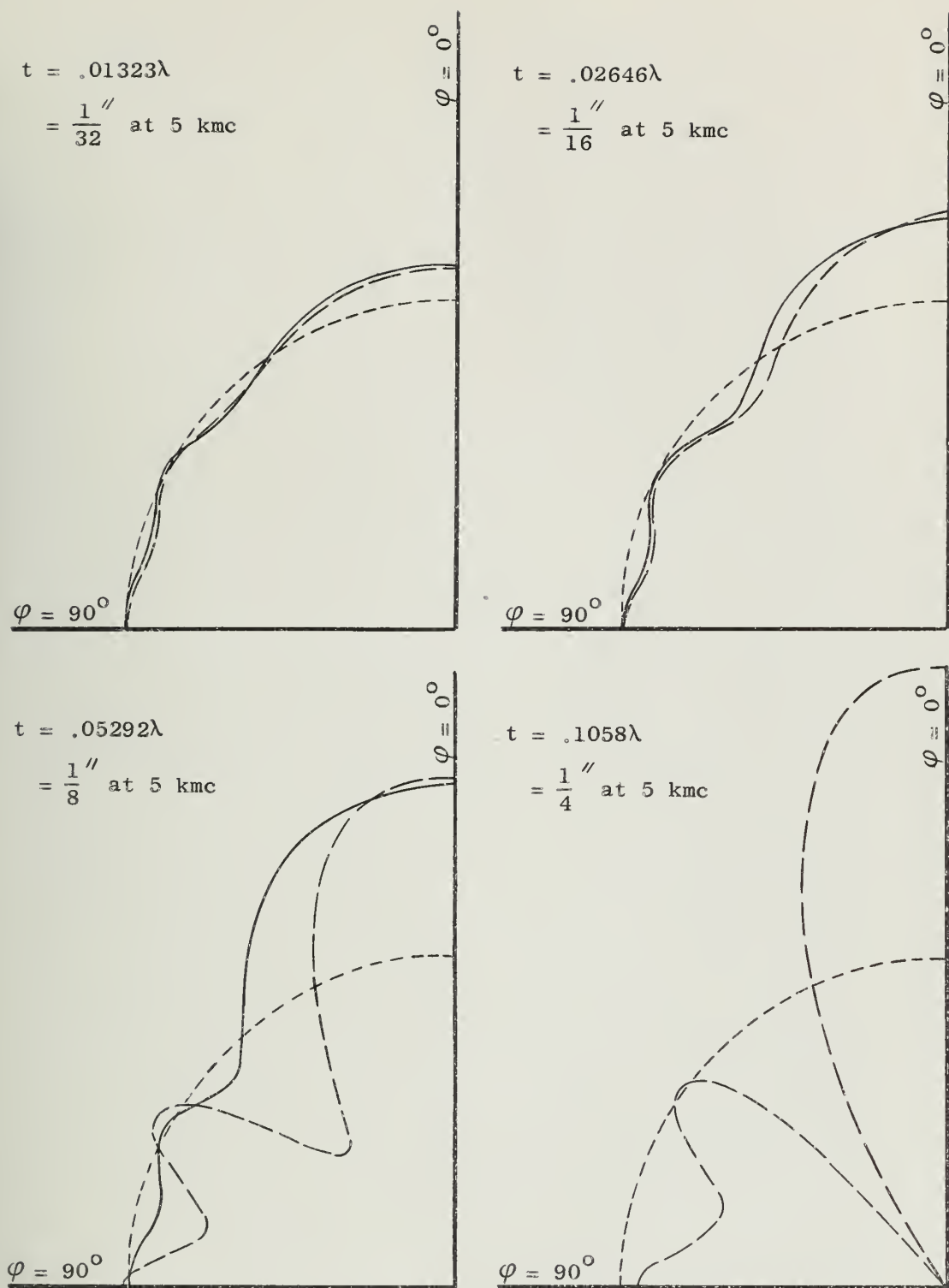


FIGURE 9. RADIATION PATTERNS: $l = 2.0\lambda$, $\epsilon_r = 2.55$

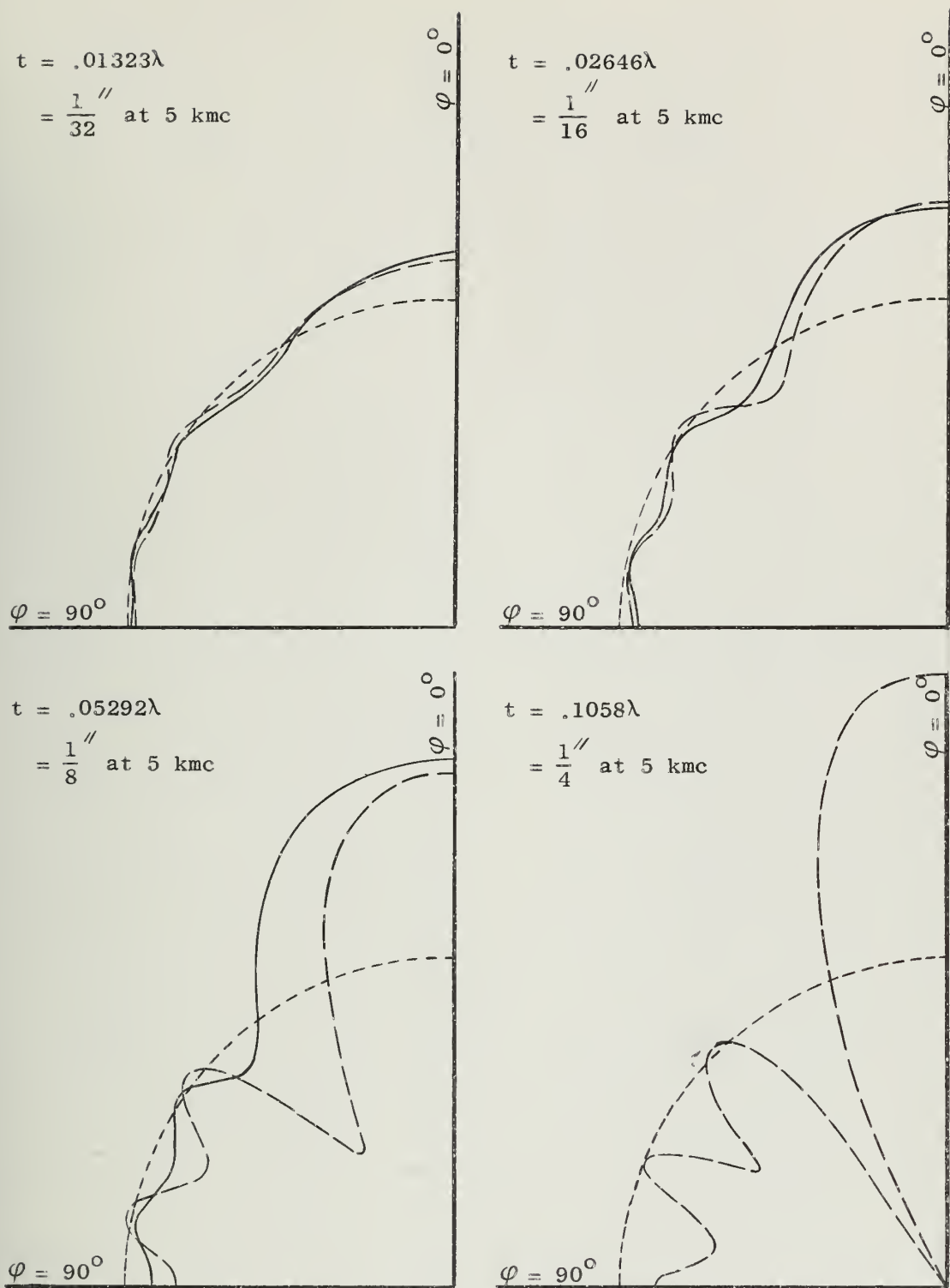


FIGURE 10. RADIATION PATTERNS: $l = 2.5\lambda$, $\epsilon_r = 2.55$

- — — — — Experimental Pattern
- — — — — Theoretical Pattern (Iteration Series)
- - - - - Unperturbed Dipole Pattern (Circle)

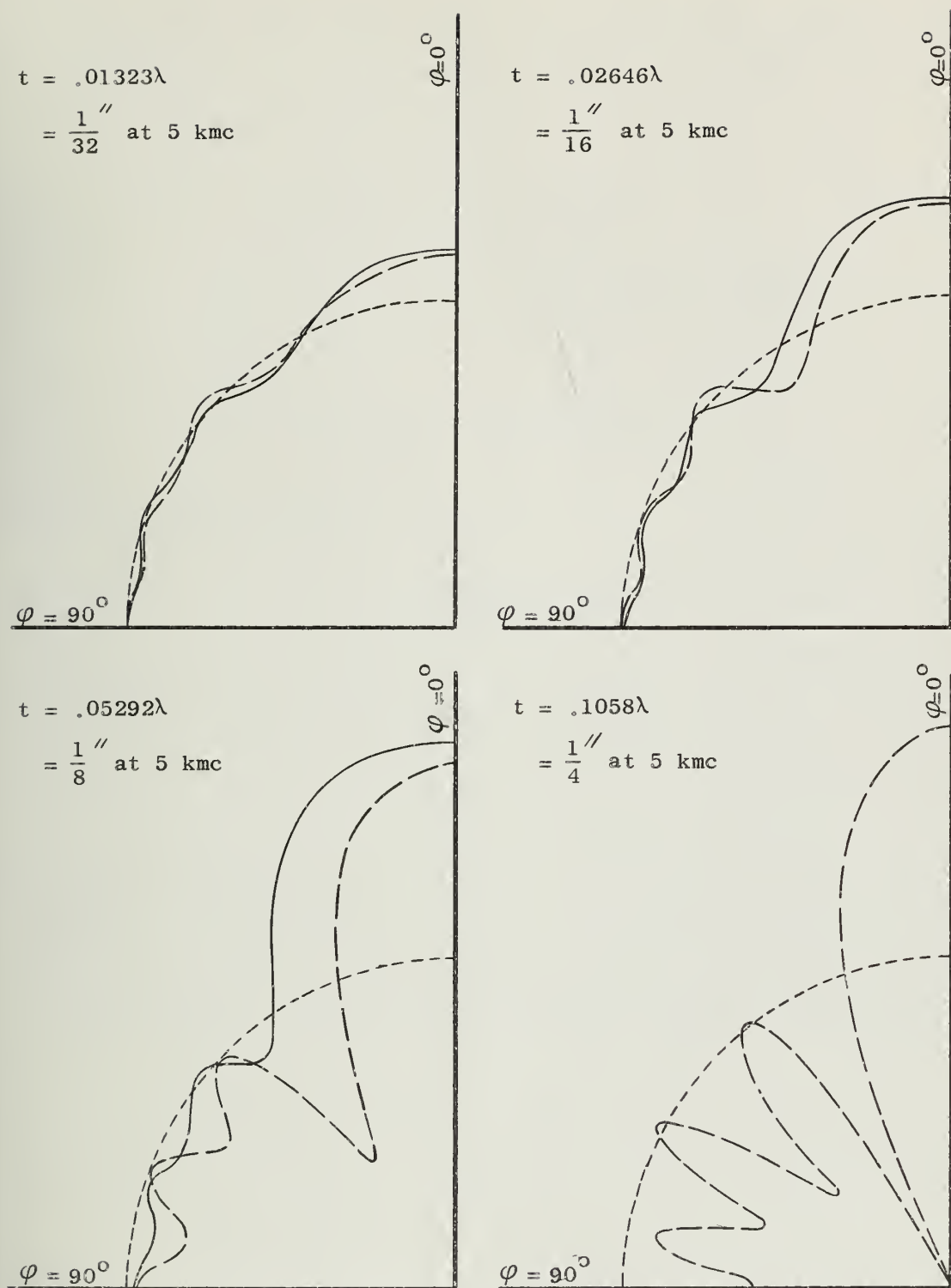


FIGURE 11. RADIATION PATTERNS: $l = 3.0\lambda$, $\epsilon_r = 2.55$

- Experimental Pattern
- Theoretical Pattern (Iteration Series)
- - - - - Unperturbed Dipole Pattern (Circle)

other nulls have roughly equal depth. This immediately suggests a means of expressing the magnitude of perturbation of the original circular dipole radiation pattern which is as follows:

Let P = unperturbed dipole pattern
(not a function of φ)

ΔP = maximum pattern perturbation or error

P_{\max} = magnitude of major lobe

P_{\min} = magnitude of principal null

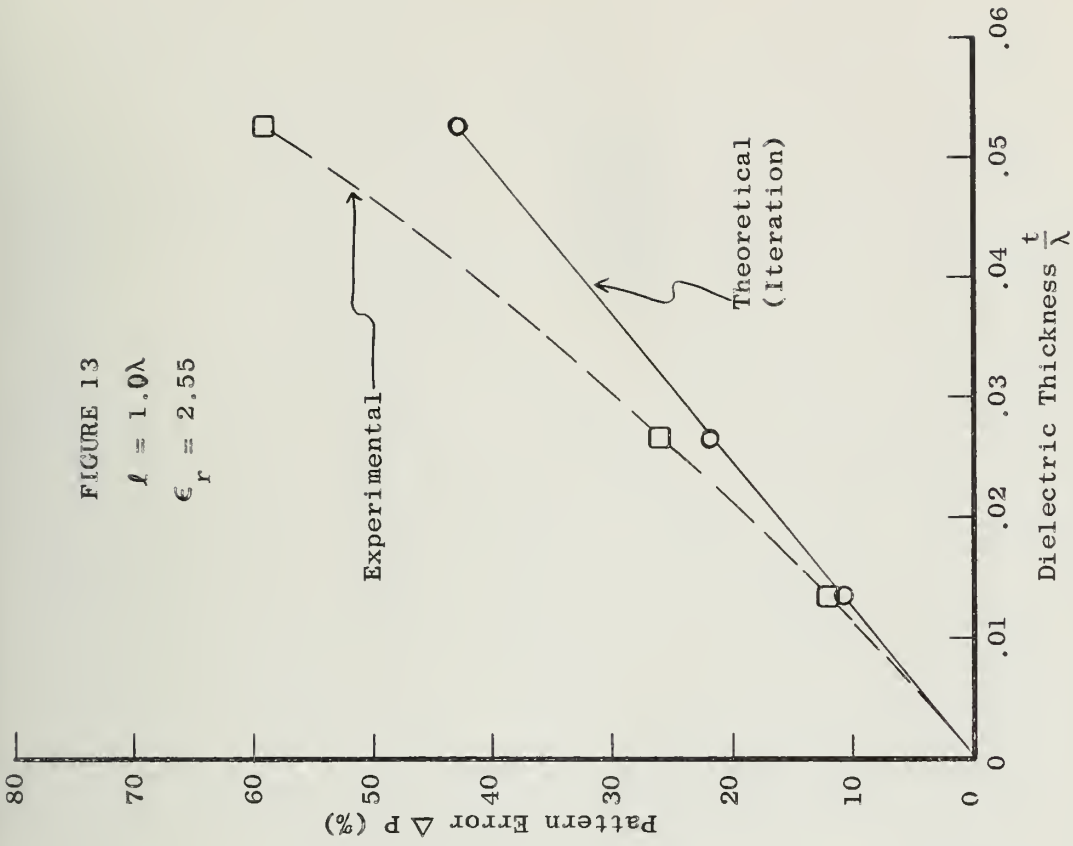
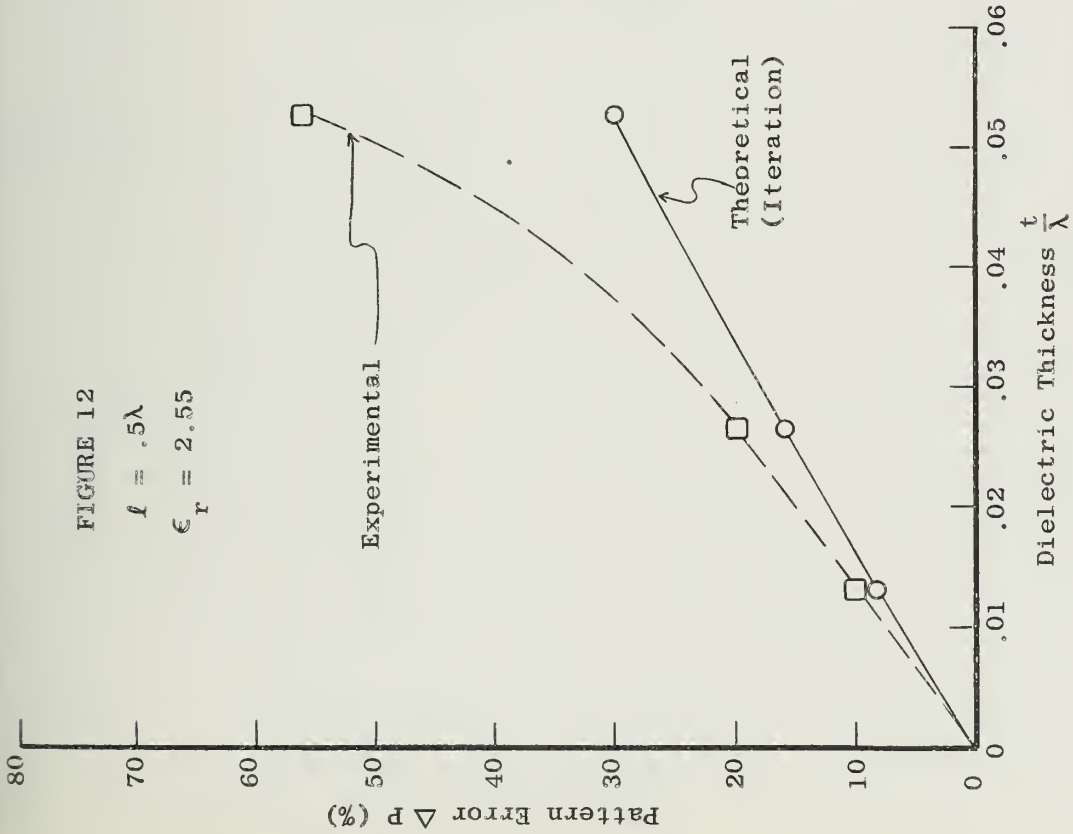
Thus ΔP is defined to be

$$\Delta P = \frac{P_{\max} - P_{\min}}{P}$$

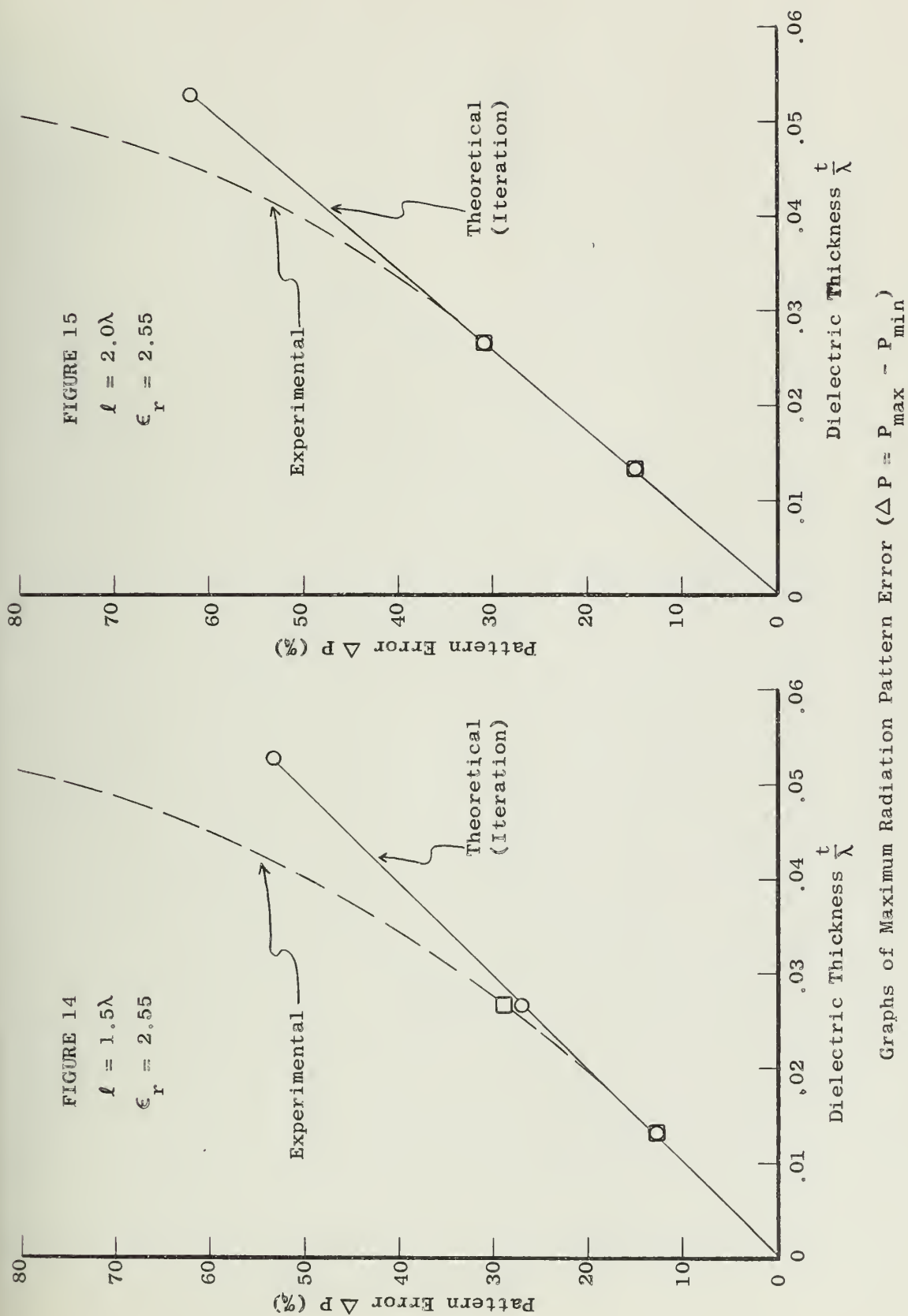
In this report P is taken to be unity so that

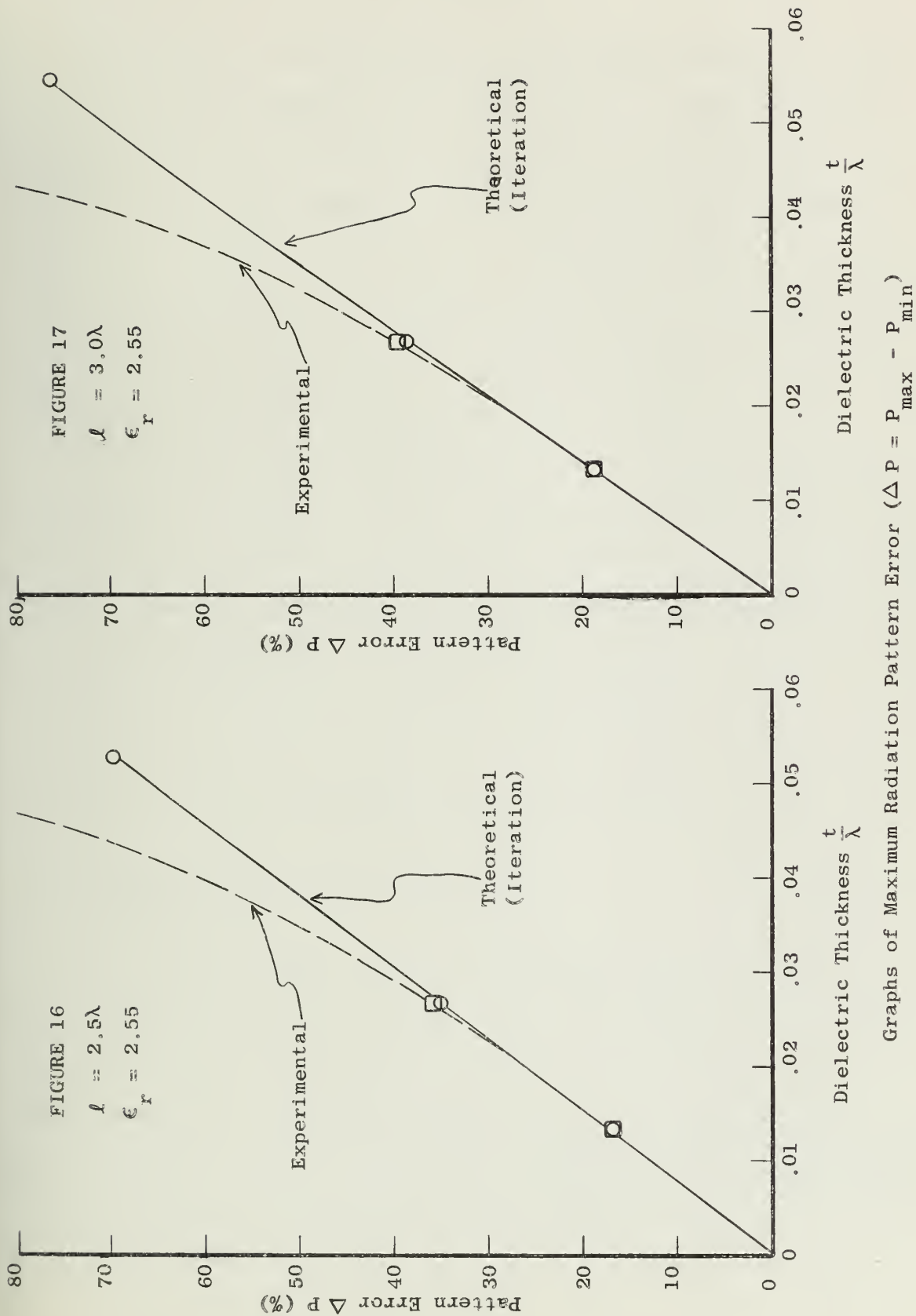
$$\Delta P = P_{\max} - P_{\min}$$

In addition, it is convenient to express ΔP as a percentage. The experimental values of ΔP are given in Figures 12 to 17 where they are compared with the theoretical values obtained from the "iteration series" solution.



Graphs of Maximum Radiation Pattern Error ($\Delta P = P_{\max} - P_{\min}$)





3. THEORY

The problem of the scattering of electromagnetic waves by a dielectric body is a very difficult one to solve and in general approximate solutions must be sought. Since approximate methods are especially useful in the solution of integral equations, it was decided to formulate the problem considered in this report as an integral equation. The method of induced sources provides a convenient means of deriving this equation and also gives some insight into the manner in which the dielectric affects the free-space radiation pattern of the metallic antenna.

The problem of scattering from an arbitrary inhomogeneous region in space can be formulated as follows. Consider the problem of determining the total electromagnetic field produced by sources \bar{J} and \bar{K} (electric and magnetic currents) in free space in the presence of an inhomogeneous region R. In free space, Maxwell's equations have the form

$$\begin{aligned}\text{curl } \bar{H} &= Y_0 \bar{E} + \bar{J} & Y_0 &= j \omega \epsilon \\ \text{curl } \bar{E} &= -Z_0 \bar{H} - \bar{K} & Z_0 &= j \omega \mu_0\end{aligned}$$

and in region R they have the form

$$\begin{aligned}\text{curl } \bar{H} &= Y_R \bar{E} & Y_R &= j \omega \epsilon_0 \epsilon_r \\ \text{curl } \bar{E} &= -Z_R \bar{H} & Z_R &= j \omega \mu_0 \mu_r\end{aligned}$$

(If polarization or conduction losses in R cannot be neglected ϵ_r and μ_r may be complex.) In order to achieve a formulation in infinite, homogeneous free space, the equations for region R can be rewritten as

$$\text{curl } \bar{H} = Y_o \bar{E} + (Y_R - Y_o) \bar{E}$$

$$\text{curl } \bar{E} = -Z_o \bar{H} - (Z_R - Z_o) \bar{H}$$

and the terms containing the differences in medium parameters can be interpreted as source terms or "induced sources". Thus the total field can be constructed by a superposition of the fields due to two sources in free space. The incident field is due to the primary sources \bar{J} and \bar{K} and the scattered field is due to the induced sources \bar{J}_i and \bar{K}_i where

$$\bar{J}_i = (Y_R - Y_o) \bar{E}$$

$$\bar{K}_i = (Z_R - Z_o) \bar{H}$$

This procedure does not lead directly to a solution of the problem since \bar{E} and \bar{H} are unknown in region R. However it does permit the formulation of the problem as an integral equation for the total field as shown by Rhodes² who considers the case of a lossless dielectric scatterer in which $\mu_r = 1$. In this case the induced current is entirely electric and has the form

$$\bar{J}_i = j \omega \epsilon_o (\epsilon_r - 1) \bar{E}$$

It is now possible to see how the dielectric scatterer perturbs the field of a metallic antenna. If the induced sources are distributed over a region in space having at least one dimension comparable to a wavelength, then they will contribute a significant amount of radiated field which is not present if the metallic antenna is located in free space. In such a case the "total" antenna is composed of dielectric as well as metal parts.

The integral equation can be specialized (as shown by Rhodes²) for the case of an infinite, cylindrical dielectric scatterer of uniform but arbitrary cross-section when the incident wave propagates in a direction normal to the cylinder axis and is polarized parallel to the axis. Appendix A shows how this integral equation can be modified for the case of an infinite line source centrally located inside an infinite dielectric cylinder having the cross-section of a long, thin rectangle. The solutions of this integral equation are derived in detail in the appendices and summarized in the remainder of this chapter.

The Iteration Series Solution

The details of this method are presented in Appendix A. In the derivation it is assumed that the dielectric sheet is thin, that its relative dielectric constant is low, that there is negligible field variation across the narrow dimension of the sheet, and that the field in the sheet is the same as the incident field in free space.

Since the experimental dipole was inserted in a small hole drilled into the edge of the dielectric sheet, it is necessary to consider a line source which is not embedded in the dielectric but rather located centrally in a small hole of radius δ . Both experimental and theoretical radiation patterns seemed quite insensitive to changes in δ provided that it was kept very small compared to a wavelength. For most of the experiments described in this report the central hole had a radius of about a hundredth of a wavelength so the value $\delta = .01\lambda$ was chosen for the calculations.

The derivation gives the following radiation pattern formula from which all the theoretical results in Figures 6 to 17 were calculated.

$$P(\varphi) = \sqrt{1 - 4KB + 4K^2(A^2 + B^2)}$$

where

$$A = \int_{.01}^{\frac{l}{\lambda}} J_0(2\pi x) \cos(2\pi x \cos \varphi) dx$$

$$B = \int_{.01}^{\frac{l}{\lambda}} N_0(2\pi x) \cos(2\pi x \cos \varphi) dx$$

$$K = \pi^2 (\epsilon_r - 1) \frac{t}{\lambda}$$

The integrals A and B are tabulated in Appendix B, together with numerical values of $P(\varphi)$.

The above formula for the radiation pattern can be simplified even further for the case of extremely thin dielectric sheets. For this case $K \ll 1$ and $K^2 \ll K$ which, together with the fact that A and B are of the order of unity, gives the following approximation for the radiation pattern.

$$P(\varphi) = 1 - 2KB$$

Thus, for extremely thin dielectric sheets, the pattern perturbations are directly proportional to $(\epsilon_r - 1) \frac{t}{\lambda}$. Furthermore $P(\varphi)$ is dependent only on B, an integral involving the Neumann function N_0 . There is only a secondary contribution from A, an integral involving the Bessel function J_0 .

The derivation summarized above (and described fully in Appendix A) gives the field at large radius due to a line source at the origin. An identical radiation pattern formula can be derived in somewhat fewer steps by applying the principle of reciprocity. This means that the radiation pattern is given by the magnitude of the electric field at the origin due to an incident plane wave coming from sources at infinity.

The Fresnel Integral Solution

This method of solving the integral equation is presented in detail in Appendix C. The assumptions involved are the same as those in the iteration series solution with two exceptions. First, in the Fresnel integral solution it is assumed that the central line source is embedded in the dielectric. This is done in order to take advantage of a very simple integral formula and is in contrast with the iteration approach which considers the line source to be in a small hole of radius δ . Second, it is assumed that the large-argument approximation for the Hankel function $H_0^{(2)}(2\pi \frac{l}{\lambda})$ is accurate even for fairly small arguments. Figure 5 shows this assumption to be valid since the approximate formula error is less than .015 if $l \geq .5\lambda$.

The basic idea in the Fresnel integral approach is that of changing the range of integration from $(-l, l)$ to a combination of $(-\infty, -l)$, (l, ∞) and $(-\infty, \infty)$. This is equivalent to breaking down the field scattered by a finite dielectric strip (from $x = -l$ to $x = l$) into the difference between the field scattered by an infinite sheet and the field scattered by two semi-infinite strips (from $x = -\infty$ to $x = -l$ and from $x = l$ to

$x = \infty$). This viewpoint gives a solution to the integral equation from which the radiation pattern $P(\varphi)$ can be obtained.

$$P(\varphi) = \left| 1 - \pi(\epsilon_r - 1) \frac{t}{\lambda} \cdot \frac{1}{\sin \varphi} \left\{ M + j(1 - N) \right\} \right|$$

where

$$M = \sin \frac{\varphi}{2} \left[S \left(\sqrt{\frac{2\gamma_1 \ell}{\pi \lambda}} \right) - C \left(\sqrt{\frac{2\gamma_1 \ell}{\pi \lambda}} \right) \right] + \cos \frac{\varphi}{2} \left[S \left(\sqrt{\frac{2\gamma_2 \ell}{\pi \lambda}} \right) - C \left(\sqrt{\frac{2\gamma_2 \ell}{\pi \lambda}} \right) \right]$$

$$N = \sin \frac{\varphi}{2} \left[1 - S \left(\sqrt{\frac{2\gamma_1 \ell}{\pi \lambda}} \right) - C \left(\sqrt{\frac{2\gamma_1 \ell}{\pi \lambda}} \right) \right] + \cos \frac{\varphi}{2} \left[1 - S \left(\sqrt{\frac{2\gamma_2 \ell}{\pi \lambda}} \right) - C \left(\sqrt{\frac{2\gamma_2 \ell}{\pi \lambda}} \right) \right]$$

$$\gamma_1 = 2\pi(1 + \cos \varphi), \quad \gamma_2 = 2\pi(1 - \cos \varphi)$$

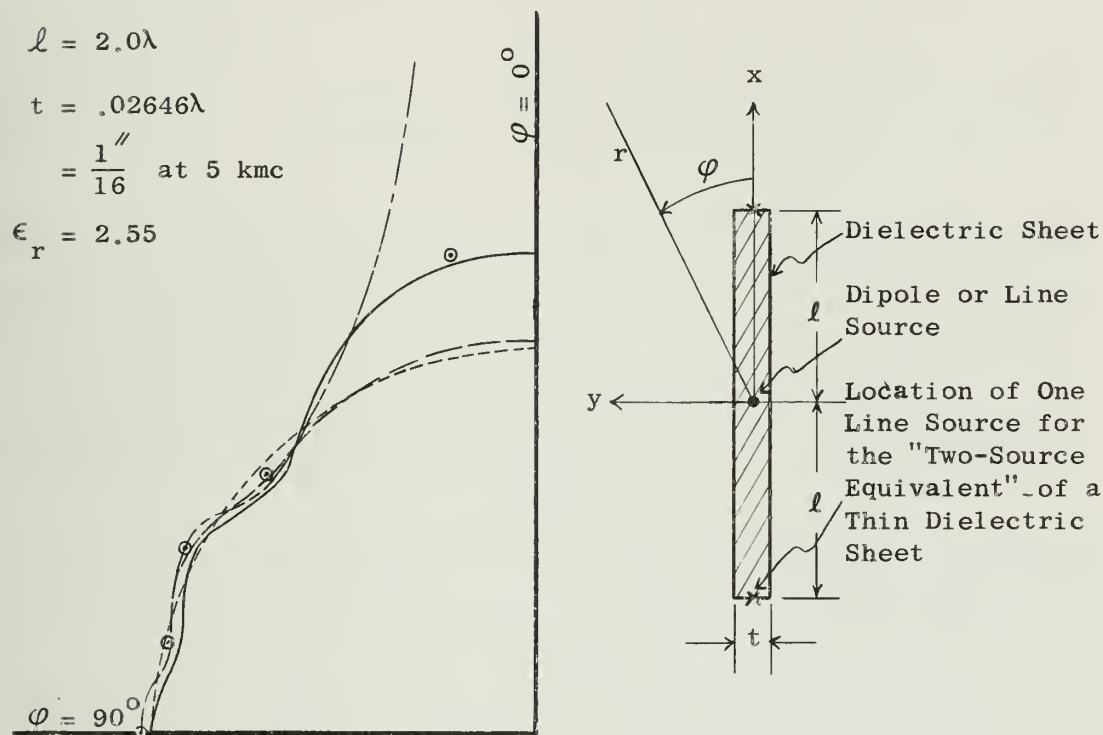
Tables⁷ of S and C are available and give S and C as functions of $\frac{\gamma_1 \ell}{\lambda}$ and $\frac{\gamma_2 \ell}{\lambda}$.

Thus the radiation patterns can be calculated in a straightforward manner without the aid of a machine computer.

Results of the iteration and Fresnel integral calculations are compared in Figure 18 for $\ell = 2.0\lambda$ and $t = .02646\lambda$. The pattern magnitudes given by the two methods differ by a small, almost constant amount (.035 approximately). This difference is believed to be due to the fact that the iteration approach considered the line source to be in a hole of radius $\delta = .01\lambda$, whereas the Fresnel integral solution takes δ to be zero. This explanation was substantially verified by some approximate calculations (iteration series method) which indicated that a pattern difference of about .03 was to be expected.

FIGURE 18

Comparison of the Iteration Series, Fresnel Integral
and "Two-Source Equivalent" Radiation Patterns



- Iteration Series (first term only)
 ○ ○ ○ ○ ○ Fresnel Integral
 - - - - - "Two-Source Equivalent" (with directivity)
 ———— "Two-Source Equivalent" (without directivity)
 - - - - - Dipole Pattern (circle of unit radius)

Pattern Magnitudes for the Iteration Series
and Fresnel Integral Solutions

ϕ	Iteration	Fresnel	Difference
10°	1.237	1.273	.036
46°	.940	.974	.034
62°	1.001	1.035	.034
76°	.956	.991	.035
90°	.991	1.025	.034

Asymptotic Behavior of the Fresnel Integral Solution

Appendix D shows that, when φ is not too close to 0° or 180° , the field at the origin P due to an incident plane wave is given by

$$E(P) = 1 + \pi(\epsilon_r - 1) \frac{t}{\lambda} \left\{ \frac{-j}{\sin \varphi} + \frac{R(\frac{\ell}{\lambda})}{2} \left[\frac{e^{-j2\pi \frac{\ell}{\lambda} \cos \varphi}}{1 + \cos \varphi} + \frac{e^{+j2\pi \frac{\ell}{\lambda} \cos \varphi}}{1 - \cos \varphi} \right] \right\}$$

where $R(\frac{\ell}{\lambda})$ is the large-argument approximation to the Hankel function $H_C^{(2)}(2\pi\frac{\ell}{\lambda})$. The factors involving $R(\frac{\ell}{\lambda})$ behave as if they were due to infinite line sources at $x = -\ell$ and $x = +\ell$ with directional characteristics $(1 + \cos \varphi)^{-1}$ and $(1 - \cos \varphi)^{-1}$ respectively and with phase factors $e^{-j2\pi \frac{\ell}{\lambda} \cos \varphi}$ and $e^{+j2\pi \frac{\ell}{\lambda} \cos \varphi}$ respectively.

Some further restrictions lead to a simple formula for the radiation pattern (the absolute value of $E(P)$). If $(\epsilon_r - 1) \frac{t}{\lambda}$ is very small, the term $(j \sin \varphi)^{-1}$ gives a negligible contribution to the radiation pattern and only the line source terms remain. Furthermore, if ℓ is some integral multiple of a half wavelength ($\ell = n \frac{\lambda}{2}$ as in the patterns in Figures 6 to 11), the radiation pattern formula becomes

$$P(\varphi) = 1 + (\epsilon_r - 1) \frac{t}{\lambda} \cdot \frac{(-1)^n}{\sqrt{n}} \left[\frac{\cos(n\pi \cos \varphi) - \cos \varphi \sin(n\pi \cos \varphi)}{\sin^2 \varphi} \right]$$

This pattern is plotted in Figure 18 for $\ell = 2.0\lambda$ ($n = 4$) and $t = .02646\lambda$.

Numerical values are as follows:

φ	$P(\varphi)$
10°	1.795
20°	1.241
30°	1.061
46°	.952
62°	1.029
76°	.978
90°	1.021

In the above expression for $P(\varphi)$, the line source directivity factors $(1 \pm \cos \varphi)^{-1}$ have been retained and the formula holds for values of φ as small as 20° .

The formula for $P(\varphi)$ can be simplified even further by considering the line sources to be non-directive. This means that $\cos \varphi \doteq 0$ and $\sin \varphi \doteq 1$. Thus φ is restricted to be fairly close to 90° . The radiation pattern formula becomes

$$P(\varphi) = 1 + (\epsilon_r - 1) \frac{t}{\lambda} \cdot \frac{(-1)^n}{\sqrt{n}} \cos(n\pi \cos \varphi)$$

This pattern is also shown in Figure 18 for $\ell = 2.0\lambda$ ($n = 4$) and $t = .02646\lambda$. Numerical values are as follows (they are taken at pattern maxima and minima):

φ	$P(\varphi)$
0°	1.021
43°	.980
62°	1.021
76°	.980
90°	1.021

In the above expression for $P(\varphi)$ the directivity of the individual line sources has been neglected. Despite this severe restriction, the formula holds fairly well for values of φ as small as 40° . In particular, the angles at which minima and maxima occur agree to within $\pm 3^\circ$ with both the experimental results and the iteration series calculations for very thin dielectric sheets.

The preceding discussion of the "two-source equivalent" has been presented because it seems to bring out two factors which help in understanding the phenomena described in this report. First, as far as radiation pattern calculations are concerned, it is more important to know the sheet length l than the exact field distribution along the sheet. Second, one can think about the problem in terms of outward-traveling cylindrical waves which are scattered at the sheet edges and nowhere else.

4. COMMENTS

There is close agreement between the "iteration series" theory and the experiments from $t = 0$ to $t = .03\lambda$ (for $\epsilon_r = 2.55$), within which range the pattern perturbations vary almost linearly with respect to sheet thickness. As t increases beyond $.03\lambda$ the theory becomes useless in that it does not predict the observed radiation patterns, especially the deep nulls. Such a breakdown of the theory is not surprising since most of the assumptions involve a very small thickness and a low dielectric constant. Improved results probably could be obtained by computing one or more additional terms in the iteration series solution for the field in the dielectric sheet.

The results reported for $\epsilon_r = 2.55$ can be extended easily to other values by use of the fact that the pattern perturbations do not depend on t alone but rather on $(\epsilon_r - 1) \frac{t}{\lambda}$. This dependence is complicated for moderately thick dielectric sheets (of the order of $\frac{\lambda}{10}$ thick) but is probably of the form

$$P(\varphi) = 1 + \left[(\epsilon_r - 1) \frac{t}{\lambda} \right] I_1 + \left[(\epsilon_r - 1) \frac{t}{\lambda} \right]^2 I_2 + \dots$$

where I_1 and I_2 are factors depending on φ and $\frac{\ell}{\lambda}$. This form is suggested by the infinite series solution which can be derived by applying the iteration technique to the integral equation. For constant length $\frac{\ell}{\lambda}$, dielectric sheets having the same value of $(\epsilon_r - 1) \frac{t}{\lambda}$ should produce nearly the same radiation pattern. Experimentally this was found to be true in the linear range where $(\epsilon_r - 1) \frac{t}{\lambda}$ is very small and approximately true even for the thickest dielectric considered in this report.

For thin dielectric sheets it is convenient to express the radiation pattern perturbation or error as

$$\Delta P = \frac{P_{\max} - P_{\min}}{P}$$

where P is the magnitude of the unperturbed, circular dipole radiation pattern. The results obtained for pattern error are higher than one might expect; that is a ΔP of 14% occurs when a dipole is laid on a square polystyrene sheet six wavelengths on a side and only a hundredth of a wavelength thick.

The theory described in this report is helpful in obtaining interpretations of the observed radiation patterns. For example, the viewpoint of induced sources results in a useful integral equation and permits the dielectric to be regarded as a distribution of electric currents in free space. This concept leads to the conclusion that a dielectric object in the near field of an antenna will alter the radiation pattern perceptibly if its size is comparable to a wavelength in at least one dimension.

Another viewpoint is that of outward-traveling cylindrical waves which are scattered only at the sheet edges. This concept suggests that the dielectric sheet may be represented approximately by line sources in free space in positions corresponding to the sheet edges. (Such a representation is well known for the problem of scattering by a metallic strip). The asymptotic approximation to the Fresnel integral formula justifies such a representation when the sheet is very thin and when

the radiation field is measured in a sector roughly perpendicular to the broad face of the sheet (φ is not close to 0° or 180°). A more accurate representation results if the individual line sources are considered to have non-circular radiation patterns.

All the calculations in this report are for a dipole source located half way between the edges of the dielectric sheet. This approach simplifies the theoretical derivations but the formulae for the radiation pattern of a dipole at any point on the sheet could be derived in a similar way. In particular, the Fresnel integral radiation pattern formula can be altered easily to fit the non-symmetrical problem. If the dielectric strip extends from $x = -l_1$ to $x = +l_2$ and if the source remains at $x = 0$, then the radiation pattern is

$$P(\varphi) = \left| 1 - \pi(\epsilon_r - 1) \frac{t}{\lambda} \cdot \frac{1}{\sin \varphi} \{M + j(1 - N)\} \right|$$

where

$$M = \sin \frac{\varphi}{2} \left[S \left(\sqrt{\frac{2\gamma_1 l_1}{\pi \lambda}} \right) - C \left(\sqrt{\frac{2\gamma_1 l_1}{\pi \lambda}} \right) \right] + \cos \frac{\varphi}{2} \left[S \left(\sqrt{\frac{2\gamma_2 l_2}{\pi \lambda}} \right) - C \left(\sqrt{\frac{2\gamma_2 l_2}{\pi \lambda}} \right) \right]$$

$$N = \sin \frac{\varphi}{2} \left[1 - S \left(\sqrt{\frac{2\gamma_1 l_1}{\pi \lambda}} \right) - C \left(\sqrt{\frac{2\gamma_1 l_1}{\pi \lambda}} \right) \right] + \cos \frac{\varphi}{2} \left[1 - S \left(\sqrt{\frac{2\gamma_2 l_2}{\pi \lambda}} \right) - C \left(\sqrt{\frac{2\gamma_2 l_2}{\pi \lambda}} \right) \right]$$

$$\gamma_1 = 2\pi(1 + \cos \varphi)$$

$$\gamma_2 = 2\pi(1 - \cos \varphi)$$

5. CONCLUSIONS

The experimental radiation patterns have been shown for the case of a dipole embedded inside a dielectric sheet (or "printed" on its surface) and these results have been found to agree with the theoretical calculations for thin sheets. The range of thickness over which theory and experiment agree is a useful range from the point of view of practical "printed circuit" antennas. As a consequence the results reported permit the antenna designer to estimate the maximum radiation pattern error likely to be encountered when mounting single dipoles or combinations of them on dielectric sheets.

The theory presented shows that a very thin dielectric strip can be regarded as being approximately equivalent to two line sources in free space in positions corresponding to the strip edges. This result is quite general and could be applied to many problems involving the scattering of electromagnetic waves by very thin dielectric sheets.

BIBLIOGRAPHY

1. Whitmer, R. M., "Radiation from a Dielectric Waveguide", Journal of Applied Physics, pp. 949-952, Vol. 23, No. 9, Sept. 1952.
2. Rhodes, D. R., "On the Theory of Scattering by Dielectric Bodies", Ohio State University Research Foundation (Antenna Laboratory), Engineering Report 475-1, July, 1953.
3. Barrar, R. B. and Dolph, C. L., "A Transmission Problem in Electromagnetic Theory", Journal of Rational Mechanics and Analysis, pp. 725-743, Vol. 3, 1954.
4. Angulo, C. M., "Diffraction of Surface Waves by a Semi-Infinite Dielectric Slab", I.R.E. Transactions on Antennas and Propagation, pp. 100-109, Vol. AP-5, No. 1, Jan. 1957.
5. Hatkin, L., "Analysis of Propagating Modes in Dielectric Sheets", Proceedings of the I.R.E., pp. 1565-1568, Vol. 42, No. 10, Oct. 1954.
6. Horton, C. W.; Karal, F. C.; McKinney, C. M., "On the Radiation Patterns of Dielectric Rods of Circular Cross Section--the TM_{01} Mode", Journal of Applied Physics, pp. 1279-1283, Vol. 21, No. 12, Dec. 1950.
7. Pearcey, T., "Table of the Fresnel Integral to Six Decimal Places", Cambridge University Press, 1956.

APPENDIX A

The Iteration Series Solution of the Integral Equation

For the case of a dielectric scatterer, the integral equation for the two-dimensional scattering problem as given by Rhodes² is

$$E_z(P) = E_z^i(P) - j \frac{(k_1^2 - k_0^2)}{4} \int_A E_z(Q) H_0^{(2)}(k_0 \rho) da$$

where

$P = (x, y)$ or (r, φ) and is the observation point

$Q = (x', y')$ or (r', φ') and is a general point inside the dielectric

$$\rho = \sqrt{(x - x')^2 + (y - y')^2}$$

$$r = \sqrt{x^2 + y^2}$$

$k_0 = \frac{2\pi}{\lambda}$ = the propagation constant in free space

$k_1 = \frac{2\pi}{\lambda} \sqrt{\epsilon_r}$ = the propagation constant in the dielectric

ϵ_r = the relative dielectric constant of the scatterer

λ = the free space wavelength

A = the cross-sectional area of the scatterer

$E_z(P)$ = the total electric field at P . ($E_x = E_y = 0$)

$E_z^i(P)$ = the incident field at P due to a two-dimensional source in free space

The above general equation must be specialized for the case of an infinite line source located centrally inside an infinite dielectric strip as shown in Figure 4. As discussed in Chapter 4, it is necessary to consider the line source as being in a hole of radius δ since the experimental dipole was inserted in such a hole drilled into the edge of the dielectric sheet. It will become evident that such a consideration avoids integrating over the Hankel function singularity at the origin. In the derivation to follow it will be understood (if not explicitly stated) that any integration over the cross-sectional area of the dielectric sheet excludes a circular region of radius δ around the line source at the origin.

If it is assumed that the dielectric sheet is very thin and that there is no field variation across it, then

$$\int_A E_z(Q) H_0^{(2)}(k_0 \rho) da = t \int_{-\ell}^{\ell} E_z(Q) H_0^{(2)}(k_0 \rho) dx'$$

where t is the sheet thickness and 2ℓ is its length. Using this relation and writing E in place of E_z , we obtain an approximate expression for the total field which is

$$E(x, y) = C H_0^{(2)}(k_0 r) - j \frac{(k^2 - k_0^2)}{4} t \int_{-\ell}^{\ell} E(x', 0) H_0^{(2)}(k_0 \rho) dx'$$

where $C H_0^{(2)}(k_0 r)$ is the field of an infinite line source located at the origin, C being a constant proportional to current strength.

Letting $y = 0$ in the above expression gives an approximate one-dimensional integral equation for the field in the dielectric sheet.

$$E(x, 0) = C H_0^{(2)}(k_0 x) - j \frac{(k_1^2 - k_0^2)}{4} t \int_{-l}^l E(x', 0) H_0^{(2)}(k_0 |x - x'|) dx'$$

If this equation is solved then the total field can be obtained from the above expression for $E(x, y)$. For the solution of this integral equation the iteration technique is to be employed. It consists of making an approximation to $E(x', 0)$, calculating $E(x, 0)$, and reinserting this function under the integral sign in place of $E(x', 0)$. By repeating this process, successively more accurate values of $E(x, 0)$ can be obtained. In other words, a series expression for $E(x, 0)$ can be derived and this series is known to converge if the coefficient preceding the integral is small enough. For these calculations it will be assumed that $E(x', 0) = 0$ which gives $E(x, 0) = C H_0^{(2)}(k_0 x)$. The iteration procedure will be carried no further than this. That is, we shall consider only the first-order term in the iteration series. This is simply a statement of the assumption that the field in the dielectric sheet is equal to the incident field in free space represented by the zero-order Hankel function. This value of $E(x', 0)$ will be inserted after some simplification of the formula for $E(x, y)$.

At this point the notation can be made somewhat more compact by expressing all lengths in terms of free space wavelengths, using bars (-) to indicate the new coordinates so that $\bar{r} = \frac{r}{\lambda}$, $\bar{x} = \frac{x}{\lambda}$ and $k_0 r = 2\pi\bar{r}$. Thus it can be seen that $\frac{1}{4}(k_1^2 - k_0^2) = \frac{\pi^2}{\lambda^2}(\epsilon_r - 1)$ and that the integral

expression for $E(x, y)$ becomes

$$E(\bar{x}, \bar{y}) = C H_0^{(2)}(2\pi\bar{r}) - j\pi^2(\epsilon_r - 1) \bar{t} \int_{-\bar{l}}^{\bar{l}} E(\bar{x}', 0) H_0^{(2)}(2\pi\bar{\rho}) d\bar{x}'$$

Setting

$$\beta = -j\pi^2(\epsilon_r - 1) \bar{t}$$

and

$$I = \int_{-\bar{l}}^{\bar{l}} E(\bar{x}', 0) H_0^{(2)}(2\pi\bar{\rho}) d\bar{x}'$$

we can put the integral expression for $E(\bar{x}, \bar{y})$ in the form

$$E(\bar{x}, \bar{y}) = C H_0^{(2)}(2\pi\bar{r}) + \beta I$$

The integral I can be transformed to an integral over the range

$0 \leq \bar{x} \leq \bar{l}$ by the following method. We have

$$I = \int_{-\bar{l}}^{\bar{l}} E(\bar{x}', 0) H_0^{(2)}(2\pi\bar{\rho}) d\bar{x}'$$

Recalling that the line source is considered to be in a hole of radius δ (or $\bar{\delta}$), we have

$$I = \int_{-\bar{l}}^{-\bar{\delta}} E(\bar{x}', 0) H_0^{(2)}(2\pi\bar{\rho}) d\bar{x}' + \int_{\bar{\delta}}^{\bar{l}} E(\bar{x}', 0) H_0^{(2)}(2\pi\bar{\rho}) d\bar{x}'$$

From the symmetry of the problem it is apparent that $E(\bar{x}', 0) = E(-\bar{x}', 0)$.

Then, writing $-\bar{x}'$ for \bar{x}' , we have

$$\begin{aligned}
 I &= \int_{\bar{\delta}}^{\bar{l}} E(-\bar{x}', 0) H_0^{(2)}[2\pi\bar{\rho}(-\bar{x}')] d\bar{x}' + \int_{\bar{\delta}}^{\bar{l}} E(\bar{x}', 0) H_0^{(2)}[2\pi\bar{\rho}(\bar{x}')] d\bar{x}' \\
 &= \int_{\bar{\delta}}^{\bar{l}} E(\bar{x}', 0) \left\{ H_0^{(2)}[2\pi\bar{\rho}(-\bar{x}')] + H_0^{(2)}[2\pi\bar{\rho}(\bar{x}')] \right\} d\bar{x}'
 \end{aligned}$$

Now a major simplification follows from the observation that $\bar{\rho}$ and \bar{r} are very large for the case of radiation field calculations. Thus the following large-argument approximations for the Hankel functions can be made.

$$H_0^{(2)}(k_0 r) = \sqrt{\frac{2}{\pi k_0 r}} e^{-j(k_0 r - \frac{\pi}{4})}$$

$$H_0^{(2)}(k_0 \rho) = \sqrt{\frac{2}{\pi k_0 \rho}} e^{-j(k_0 \rho - \frac{\pi}{4})}$$

If r and ρ are large, we can set $\rho = r$ in the amplitude factor and

$\rho = r - x \cos \varphi$ in the phase factor so that

$$H_0^{(2)}(k_0 \rho) = \sqrt{\frac{2}{\pi k_0 r}} e^{-j(k_0 r - \frac{\pi}{4})} \cdot e^{jk_0 x \cos \varphi}$$

Using the barred notation, the Hankel function approximations are given

by

$$H_0^{(2)}(2\pi\bar{r}) = \frac{1}{\pi\sqrt{\bar{r}}} e^{-j(2\pi\bar{r} - \frac{\pi}{4})}$$

$$H_0^{(2)}(2\pi\bar{\rho}) = \frac{1}{\pi\sqrt{\bar{r}}} e^{-j(2\pi\bar{r} - \frac{\pi}{4})} \cdot e^{j2\pi\bar{x} \cos \varphi}$$

Introducing the above large-argument approximations, we have

$$\begin{aligned} I &= \int_{\bar{\delta}}^{\bar{\ell}} E(\bar{x}', 0) \frac{1}{\pi\sqrt{\bar{r}}} e^{-j(2\pi\bar{r} - \frac{\pi}{4})} \left\{ e^{j2\pi\bar{x}' \cos \varphi} + e^{-j2\pi\bar{x}' \cos \varphi} \right\} d\bar{x}' \\ &= \int_{\bar{\delta}}^{\bar{\ell}} E(\bar{x}', 0) \frac{1}{\pi\sqrt{\bar{r}}} e^{-j(2\pi\bar{r} - \frac{\pi}{4})} \cdot 2 \cos(2\pi\bar{x}' \cos \varphi) d\bar{x}' \\ &= \int_{\bar{\delta}}^{\bar{\ell}} E(\bar{x}', 0) N(\bar{r}, \bar{x}', \varphi) d\bar{x}' \end{aligned}$$

where

$$N(\bar{r}, \bar{x}', \varphi) = R(\bar{r}) X(\bar{x}', \varphi)$$

$$R(\bar{r}) = \frac{1}{\pi\sqrt{\bar{r}}} e^{-j(2\pi\bar{r} - \frac{\pi}{4})}$$

$$X(\bar{x}', \varphi) = 2 \cos(2\pi\bar{x}' \cos \varphi)$$

The problem can now be stated entirely in a polar coordinate system in which $E(\bar{x}, \bar{y})$ becomes $E(\bar{r}, \varphi)$ and $E(\bar{x}', \bar{y}')$ becomes $E(\bar{r}', \varphi')$. In simplified form the integral expression for the radiation field is

$$E(\bar{r}, \varphi) = C R(\bar{r}) + \beta \int_{\bar{\delta}}^{\bar{\ell}} E(\bar{r}', 0) N(\bar{r}, \bar{r}', \varphi) d\bar{r}'$$

The above relation will permit a calculation of $E(\bar{r}, \varphi)$ provided that $E(\bar{r}', 0)$ is known. The field in the dielectric sheet is unknown for all cases except the case of an infinitely thin sheet with a low dielectric constant. For that case the field in the sheet will be approximately equal to the incident field in free space. That is we can set $E(\bar{r}', 0) = CH_0^{(2)}(2\pi\bar{r}')$, an approximation already shown to be equivalent to the use of the first order approximate solution of the integral equation for the field inside the dielectric sheet. Thus we have

$$\begin{aligned} E(\bar{r}, \varphi) &= C R(\bar{r}) + \beta R(\bar{r}) C \int_{\bar{\delta}}^{\bar{\ell}} H_0^{(2)}(2\pi\bar{r}') X(\bar{r}', \varphi) d\bar{r}' \\ &= C R(\bar{r}) \left[1 + \beta \int_{\bar{\delta}}^{\bar{\ell}} H_0^{(2)}(2\pi\bar{r}') X(\bar{r}', \varphi) d\bar{r}' \right] \end{aligned}$$

and the radiation pattern $P(\varphi)$ is given by

$$P(\varphi) = \left| 1 + \beta \int_{\bar{\delta}}^{\bar{\ell}} H_0^{(2)}(2\pi\bar{r}') X(\bar{r}', \varphi) d\bar{r}' \right|$$

The variable \bar{r}' is just a variable of integration so the notation can be simplified by writing x in place of \bar{r}' . The pattern expression becomes

$$P(\varphi) = \left| 1 + \beta \int_{\bar{\delta}}^{\bar{\ell}} H_0^{(2)}(2\pi x) X(x, \varphi) dx \right|$$

$$= \left| 1 + 2\beta \left\{ \int_{\bar{\delta}}^{\bar{\ell}} J_0(2\pi x) \cos(2\pi x \cos \varphi) dx - j \int_{\bar{\delta}}^{\bar{\ell}} N_0(2\pi x) \cos(2\pi x \cos \varphi) dx \right\} \right|$$

Setting

$$A = \int_{\bar{\delta}}^{\bar{\ell}} J_0(2\pi x) \cos(2\pi x \cos \varphi) dx$$

$$B = \int_{\bar{\delta}}^{\bar{\ell}} N_0(2\pi x) \cos(2\pi x \cos \varphi) dx$$

we have

$$P(\varphi) = \left| 1 + 2\beta(A - jB) \right|$$

Setting $\beta = -jK$ and $K = \pi^2(\epsilon_r - 1)\bar{t}$, we have

$$P(\varphi) = \left| 1 - 2KB - j2KA \right| = \sqrt{(1 - 2KB)^2 + (2KA)^2} = \sqrt{1 - 4KB + 4K^2(A^2 + B^2)}$$

This is the required approximate radiation pattern formula. The value of $\bar{\delta}$ was set at .01 since in the experimental work the monopole was inserted in a hole having a radius of about a hundredth of a wavelength. The above

results are summarized in Chapter 3 and numerical calculations are tabulated in Appendix B.

APPENDIX B

Numerical Results

The numerical results of the radiation pattern calculations are contained in the following pages. The calculations given are for the iteration series solution of the integral equation and the polar graphs of these values are shown in Figures 6 to 11.

Also included are numerical values for the integrals

$$A = \int_{.01}^{\frac{\ell}{\lambda}} J_0(2\pi x) \cos(2\pi x \cos \varphi) dx$$

$$B = \int_{.01}^{\frac{\ell}{\lambda}} N_0(2\pi x) \cos(2\pi x \cos \varphi) dx$$

Radiation Patterns - Table 1

ϕ°	$t = .01323\lambda$		$\epsilon_r = 2.55$			
	$\ell = .5\lambda$	$\ell = 1.0\lambda$	$\ell = 1.5\lambda$	$\ell = 2.0\lambda$	$\ell = 2.5\lambda$	$\ell = 3.0\lambda$
0	1.057	1.083	1.103	1.121	1.136	1.150
2	1.056	1.083	1.103	1.121	1.136	1.150
4	1.056	1.083	1.103	1.120	1.135	1.148
6	1.056	1.082	1.102	1.118	1.132	1.145
8	1.056	1.081	1.100	1.116	1.129	1.141
10	1.055	1.080	1.098	1.113	1.125	1.135
12	1.055	1.079	1.096	1.109	1.120	1.128
14	1.054	1.077	1.093	1.104	1.113	1.119
16	1.054	1.075	1.089	1.098	1.105	1.108
18	1.053	1.073	1.085	1.092	1.095	1.095
20	1.052	1.070	1.080	1.084	1.084	1.080
22	1.051	1.067	1.074	1.075	1.071	1.063
24	1.050	1.064	1.068	1.065	1.057	1.045
26	1.048	1.060	1.060	1.054	1.042	1.027
28	1.047	1.056	1.053	1.042	1.026	1.008
30	1.045	1.051	1.044	1.030	1.011	.991
32	1.043	1.046	1.036	1.017	.996	.977
34	1.042	1.041	1.026	1.005	.983	.966
36	1.040	1.035	1.017	.994	.973	.960
38	1.037	1.030	1.008	.984	.966	.959
40	1.035	1.024	.999	.975	.962	.963
42	1.033	1.017	.991	.969	.963	.971
44	1.030	1.011	.984	.966	.966	.980
46	1.027	1.005	.978	.965	.973	.990
48	1.024	.999	.973	.967	.981	.996
50	1.022	.994	.970	.971	.988	.999
52	1.019	.989	.969	.976	.995	.998
54	1.015	.984	.969	.983	.998	.993
56	1.012	.980	.971	.989	.999	.986
58	1.009	.977	.974	.994	.996	.979
60	1.006	.975	.978	.998	.991	.974
62	1.003	.973	.983	.999	.985	.972
64	1.000	.973	.988	.998	.979	.975
66	.997	.973	.992	.995	.975	.980
68	.994	.974	.996	.991	.974	.986
70	.991	.976	.998	.986	.975	.991
72	.988	.979	.999	.981	.979	.992
74	.986	.981	.998	.977	.985	.989
76	.983	.985	.997	.976	.989	.984
78	.981	.988	.994	.976	.992	.978
80	.980	.991	.990	.978	.993	.975
82	.978	.994	.986	.982	.990	.975
84	.977	.997	.982	.986	.986	.979
86	.976	.999	.979	.991	.981	.984
88	.976	1.000	.977	.993	.977	.988
90	.976	1.000	.977	.994	.976	.990

ϕ°	$t = .02646\lambda$		$\epsilon_r = 2.55$			
	$\ell = .5\lambda$	$\ell = 1.0\lambda$	$\ell = 1.5\lambda$	$\ell = 2.0\lambda$	$\ell = 2.5\lambda$	$\ell = 3.0\lambda$
0	1.116	1.172	1.215	1.252	1.285	1.315
2	1.116	1.171	1.215	1.251	1.284	1.314
4	1.115	1.171	1.213	1.250	1.282	1.311
6	1.115	1.170	1.212	1.247	1.278	1.306
8	1.114	1.168	1.209	1.243	1.273	1.299
10	1.114	1.166	1.205	1.237	1.265	1.289
12	1.113	1.163	1.201	1.230	1.255	1.276
14	1.111	1.160	1.195	1.222	1.243	1.259
16	1.110	1.157	1.188	1.211	1.228	1.239
18	1.109	1.152	1.180	1.199	1.210	1.215
20	1.107	1.147	1.171	1.184	1.189	1.187
22	1.105	1.142	1.160	1.167	1.165	1.155
24	1.102	1.135	1.148	1.148	1.138	1.120
26	1.100	1.128	1.135	1.127	1.109	1.083
28	1.097	1.120	1.120	1.104	1.078	1.045
30	1.094	1.111	1.104	1.080	1.047	1.009
32	1.091	1.102	1.087	1.055	1.016	.977
34	1.087	1.092	1.069	1.031	.988	.952
36	1.083	1.081	1.050	1.007	.965	.936
38	1.079	1.070	1.032	.985	.947	.930
40	1.074	1.058	1.014	.967	.937	.935
42	1.070	1.046	.997	.953	.935	.948
44	1.065	1.034	.982	.943	.940	.965
46	1.059	1.021	.968	.940	.951	.983
48	1.054	1.010	.958	.941	.965	.996
50	1.048	.998	.950	.947	.980	1.003
52	1.042	.988	.946	.957	.992	1.001
54	1.036	.978	.945	.969	1.000	.992
56	1.030	.970	.948	.981	1.002	.978
58	1.024	.963	.953	.991	.997	.964
60	1.018	.958	.961	.998	.988	.953
62	1.012	.954	.969	1.001	.976	.950
64	1.005	.952	.978	.999	.965	.954
66	.999	.952	.987	.994	.956	.964
68	.994	.954	.994	.986	.953	.975
70	.988	.957	.998	.976	.955	.984
72	.983	.961	1.000	.967	.962	.986
74	.978	.967	.999	.960	.972	.981
76	.974	.973	.996	.956	.981	.972
78	.970	.979	.990	.957	.987	.961
80	.967	.985	.983	.961	.987	.955
82	.964	.991	.976	.968	.983	.955
84	.961	.996	.969	.976	.974	.961
86	.960	1.000	.963	.984	.965	.971
88	.959	1.002	.960	.989	.959	.979
90	.959	1.003	.958	.991	.956	.983

ϕ	$t = .05292\lambda$		$\epsilon_r = 2.55$			
	$\ell = .5\lambda$	$\ell = 1.0\lambda$	$\ell = 1.5\lambda$	$\ell = 2.0\lambda$	$\ell = 2.5\lambda$	$\ell = 3.0\lambda$
0	1.24	1.361	1.455	1.535	1.606	1.671
2	1.241	1.360	1.454	1.534	1.605	1.669
4	1.240	1.359	1.452	1.531	1.601	1.665
6	1.240	1.357	1.449	1.526	1.595	1.657
8	1.238	1.355	1.444	1.520	1.586	1.645
10	1.237	1.351	1.438	1.510	1.573	1.629
12	1.235	1.347	1.430	1.499	1.557	1.607
14	1.233	1.341	1.421	1.484	1.536	1.580
16	1.231	1.335	1.409	1.466	1.511	1.546
18	1.228	1.327	1.395	1.444	1.480	1.505
20	1.224	1.318	1.379	1.419	1.444	1.456
22	1.220	1.308	1.360	1.389	1.402	1.400
24	1.216	1.296	1.338	1.356	1.354	1.336
26	1.211	1.283	1.314	1.318	1.300	1.266
28	1.206	1.269	1.287	1.276	1.243	1.192
30	1.201	1.253	1.258	1.231	1.182	1.118
32	1.194	1.236	1.227	1.184	1.120	1.046
34	1.188	1.217	1.193	1.136	1.060	.984
36	1.180	1.197	1.158	1.087	1.005	.936
38	1.172	1.176	1.122	1.041	.960	.909
40	1.164	1.154	1.087	.999	.927	.904
42	1.155	1.132	1.052	.963	.910	.920
44	1.146	1.108	1.019	.935	.909	.949
46	1.136	1.085	.989	.919	.923	.981
48	1.126	1.062	.964	.913	.947	1.008
50	1.115	1.040	.943	.919	.974	1.022
52	1.104	1.018	.929	.933	.998	1.022
54	1.093	.998	.922	.952	1.014	1.007
56	1.081	.980	.921	.974	1.019	.983
58	1.070	.965	.927	.993	1.012	.956
60	1.058	.952	.938	1.007	.997	.933
62	1.046	.942	.952	1.013	.976	.922
64	1.035	.936	.968	1.012	.955	.925
66	1.024	.932	.983	1.003	.937	.941
68	1.013	.932	.996	.989	.928	.961
70	1.003	.936	1.005	.973	.929	.978
72	.993	.942	1.010	.956	.939	.983
74	.984	.950	1.009	.943	.956	.975
76	.976	.960	1.003	.935	.972	.959
78	.969	.971	.994	.934	.983	.941
80	.962	.981	.982	.939	.984	.929
82	.957	.992	.969	.950	.977	.927
84	.953	1.000	.957	.964	.963	.937
86	.950	1.007	.948	.977	.947	.953
88	.948	1.011	.941	.987	.936	.968
90	.947	1.013	.939	.991	.931	.974

Integrals - Table 4

φ°	$\ell = .5\lambda$		$\ell = 1.0\lambda$	
	A	B	A	B
0	.14039	-.13587	.20639	-.19708
2	.14048	-.13575	.20666	-.19678
4	.14076	-.13541	.20748	-.19585
6	.14121	-.13482	.20882	-.19429
8	.14184	-.13401	.21068	-.19208
10	.14265	-.13294	.21302	-.18919
12	.14362	-.13163	.21582	-.18557
14	.14476	-.13005	.21904	-.18120
16	.14606	-.12820	.22262	-.17602
18	.14750	-.12607	.22650	-.16999
20	.14909	-.12364	.23063	-.16307
22	.15080	-.12091	.23493	-.15523
24	.15264	-.11786	.23931	-.14642
26	.15458	-.11447	.24367	-.13665
28	.15663	-.11075	.24793	-.12591
30	.15875	-.10668	.25197	-.11422
32	.16095	-.10225	.25567	-.10163
34	.16320	-.09745	.25893	-.08821
36	.16549	-.09230	.26162	-.07408
38	.16780	-.08677	.26365	-.05937
40	.17013	-.08090	.26489	-.04427
42	.17246	-.07467	.26525	-.02897
44	.17476	-.06811	.26464	-.01371
46	.17704	-.06124	.26300	.00122
48	.17926	-.05408	.26027	.01556
50	.18143	-.04667	.25644	.02900
52	.18353	-.03904	.25149	.04124
54	.18554	-.03123	.24545	.05200
56	.18746	-.02329	.23839	.06102
58	.18929	-.01529	.23037	.06808
60	.19101	-.00727	.22152	.07302
62	.19261	.00070	.21196	.07574
64	.19410	.00855	.20186	.07622
66	.19547	.01620	.19140	.07453
68	.19673	.02360	.18076	.07081
70	.19786	.03066	.17015	.06532
72	.19888	.03732	.15977	.05837
74	.19977	.04350	.14983	.05034
76	.20056	.04913	.14052	.04170
78	.20123	.05415	.13203	.03289
80	.20179	.05851	.12454	.02441
82	.20224	.06214	.11820	.01673
84	.20259	.06502	.11312	.01026
86	.20284	.06710	.10942	.00537
88	.20299	.06836	.10717	.00232
90	.20304	.06878	.10642	.00129

Integrals - Table 5

ϕ°	$\ell = 1.5\lambda$		$\ell = 2.0\lambda$	
	A	B	A	B
0	.25570	-.24359	.29663	-.28261
2	.25621	-.24304	.29742	-.28176
4	.25773	-.24137	.29977	-.27921
6	.26022	-.23855	.30362	-.27487
8	.26364	-.23451	.30885	-.26865
10	.26792	-.22920	.31532	-.26038
12	.27295	-.22250	.32279	-.24991
14	.27860	-.21434	.33101	-.23707
16	.28474	-.20460	.33962	-.22169
18	.29117	-.19322	.34824	-.20367
20	.29769	-.18011	.35639	-.18296
22	.30407	-.16524	.36355	-.15961
24	.31002	-.14863	.36916	-.13382
26	.31527	-.13034	.37263	-.10594
28	.31951	-.11051	.37340	-.07653
30	.32245	-.08938	.37092	-.04632
32	.32378	-.06727	.36479	-.01625
34	.32321	-.04460	.35471	.01257
36	.32053	-.02186	.34061	.03894
38	.31553	.00032	.32264	.06164
40	.30813	.02133	.30125	.07951
42	.29829	.04046	.27715	.09163
44	.28612	.05704	.25133	.09740
46	.27182	.07045	.22502	.09674
48	.25570	.08019	.19958	.09007
50	.23822	.08591	.17639	.07842
52	.21990	.08746	.15676	.06334
54	.20135	.08498	.14173	.04681
56	.18326	.07883	.13202	.03097
58	.16628	.06966	.12782	.01792
60	.15106	.05833	.12883	.00937
62	.13818	.04592	.13422	.00638
64	.12809	.03358	.14270	.00919
66	.12110	.02245	.15269	.01711
68	.11734	.01357	.16246	.02861
70	.11676	.00778	.17037	.04154
72	.11911	.00557	.17513	.05351
74	.12397	.00708	.17587	.06233
76	.13076	.01205	.17236	.06639
78	.13879	.01982	.16501	.06502
80	.14731	.02941	.15478	.05861
82	.15558	.03967	.14311	.04856
84	.16286	.04933	.13164	.03701
86	.16855	.05722	.12203	.02643
88	.17216	.06238	.11563	.01901
90	.17340	.06417	.11339	.01635

φ°	$\ell = 2.5\lambda$		$\ell = 3.0\lambda$	
	A	B	A	B
0	.33228	-.31686	.36421	-.34776
2	.33339	-.31569	.36569	-.34622
4	.33669	-.31212	.37002	-.34155
6	.34205	-.30606	.37705	-.33356
8	.34929	-.29731	.38643	-.32196
10	.35812	-.28561	.39773	-.30638
12	.36813	-.27072	.41027	-.28645
14	.37882	-.25237	.42324	-.26184
16	.38959	-.23037	.43560	-.23234
18	.39967	-.20462	.44618	-.19797
20	.40824	-.17521	.45359	-.15914
22	.41436	-.14245	.45644	-.11665
24	.41708	-.10696	.45341	-.07185
26	.41550	-.06968	.44335	-.02666
28	.40882	-.03193	.42555	.01651
30	.39649	.00471	.39992	.05493
32	.37831	.03835	.36714	.08578
34	.35453	.06706	.32883	.10663
36	.32588	.08900	.28746	.11585
38	.29369	.10273	.24624	.11309
40	.25975	.10744	.20873	.09957
42	.22627	.10320	.17836	.07824
44	.19562	.09111	.15780	.05345
46	.17003	.07330	.14834	.03026
48	.15136	.05275	.14954	.01351
50	.14067	.03290	.15906	.00667
52	.13809	.01713	.17301	.01085
54	.14264	.00810	.18670	.02434
56	.15231	.00724	.19562	.04294
58	.16438	.01430	.19658	.06094
60	.17578	.02739	.18858	.07284
62	.18369	.04325	.17318	.07508
64	.18603	.05797	.15408	.06735
66	.18195	.06795	.13609	.05278
68	.17194	.07080	.12377	.03695
70	.15781	.06602	.11994	.02584
72	.14234	.05520	.12478	.02362
74	.12856	.04158	.13569	.03087
76	.11920	.02923	.14821	.04434
78	.11595	.02178	.15744	.05826
80	.11913	.02139	.15978	.06664
82	.12754	.02806	.15413	.06598
84	.13883	.03955	.14235	.05671
86	.14996	.05217	.12855	.04309
88	.15805	.06184	.11764	.03128
90	.16101	.06545	.11351	.02665

APPENDIX C

The Fresnel Integral Solution

This approach makes use of the integral equation described at the beginning of Appendix A.

$$E(P) = E^i(P) - j \frac{(k^2 - k_o^2)}{4} \int_A E(Q) H_o^{(2)}(k_o \rho) da$$

For the iteration series solution, the field at a distant point P was calculated, using the infinite line source at the origin as the primary source. For the following calculations the principle of reciprocity will be employed merely to illustrate that there exist two equivalent view-points from which the same radiation pattern formulation may be obtained. For the reciprocal case, the quantity to be obtained becomes the electric field at the origin due to an incident plane wave. In other words the point P will be taken to be the origin and the field in the dielectric sheet $[E(Q)]$ will be due to the incident plane wave. The radiation pattern is thus given by the absolute value of $E(P)$.

As in Appendix A, it will be assumed that the dielectric sheet is very thin so that the integral over its cross-section can be replaced by its thickness multiplied by the line integral along the sheet. Furthermore it will be assumed (also as in Appendix A) that the field inside the sheet is the same as the incident field in free space. The incident field E^i is a plane wave with arbitrary phase and magnitude. It is convenient to choose the phase and magnitude so that the field at the origin

has unit magnitude and zero phase angle, that is $E^i(P) = 1$. This gives the electric field along the sheet: $E(Q) = e^{jk_0 x' \cos \varphi}$. It must also be observed that ρ (the distance between P and Q) is now $|x|$ so that $H_0^{(2)}(k_0 \rho)$ becomes $H_0^{(2)}(k_0 |x'|)$.

The notation in the remainder of the derivation will be made slightly more compact if all distances are in free-space wavelengths (indicated by a bar over the distance symbol). That is $\bar{x} = \frac{x}{\lambda}$, $\bar{l} = \frac{l}{\lambda}$, $e^{jk_0 x' \cos \varphi} = e^{j2\pi \bar{x}' \cos \varphi}$, and $H_0^{(2)}(k_0 |x'|) = H_0^{(2)}(2\pi |\bar{x}'|)$.

Now we can write the integral relation giving the field at the origin P due to an incident plane wave.

$$E(P) = 1 - j\pi^2(\epsilon_r - 1) \bar{t} \int_{-\bar{l}}^{\bar{l}} e^{j2\pi \bar{x}' \cos \varphi} H_0^{(2)}(2\pi |\bar{x}'|) d\bar{x}'$$

The primes (previously used to indicate coordinates in the dielectric sheet) can now be dropped since there are no unprimed coordinates in the formula.

So far the procedure has been essentially equivalent to that used in the iteration series approach. Now, in order to make use of the Fresnel integrals, it is necessary to write the above equation in the form

$$E(P) = 1 - j\pi^2(\epsilon_r - 1) \bar{t} \left[\int_{-\infty}^{\infty} e^{j2\pi \bar{x} \cos \varphi} H_0^{(2)}(2\pi |\bar{x}|) d\bar{x} - \int_{-\infty}^{-\bar{l}} e^{j2\pi \bar{x} \cos \varphi} H_0^{(2)}(2\pi |\bar{x}|) d\bar{x} - \int_{\bar{l}}^{\infty} e^{j2\pi \bar{x} \cos \varphi} H_0^{(2)}(2\pi |\bar{x}|) d\bar{x} \right]$$

This can be written as $E(P) = 1 + E_1(P) - E_2(P)$ where $E_1(P)$ is the field due to an infinite dielectric sheet and $E_2(P)$ is due to a pair of semi-infinite sheets (one from $-\bar{l}$ to $-\infty$ and the other from $+l$ to $+\infty$).

Calculation of $E_1(P)$

If we set $\beta = -j\pi^2(\epsilon_r - 1)\bar{t}$, we have

$$\begin{aligned} E_1(P) &= \beta \int_{-\infty}^{\infty} H_0^{(2)}(2\pi|\bar{x}|) e^{j2\pi\bar{x} \cos \varphi} d\bar{x} \\ &= 2\beta \int_0^{\infty} H_0^{(2)}(2\pi\bar{x}) \cos(2\pi\bar{x} \cos \varphi) d\bar{x} \end{aligned}$$

Setting $u = 2\pi\bar{x}$, we can write

$$E_1(P) = \frac{\beta}{\pi} \int_0^{\infty} H_0^{(2)}(u) \cos(u \cos \varphi) du$$

It is worth noting that the range of integration is from zero to infinity. In the iteration series derivation, the integration did not start from zero but from a small value δ . This took into account the fact that the experimental dipole was inserted in a hole of radius δ . For the derivation to follow, the hole will not be considered ($\delta = 0$) in order to take advantage of the following integral formulae:

$$\int_0^{\infty} J_0(ax) \cos(bx) dx = \frac{1}{\sqrt{a^2 - b^2}} \quad 0 < b < a$$

$$= \infty \quad b = a$$

$$= 0 \quad a < b < \infty$$

$$\int_0^{\infty} N_0(ax) \cos(bx) dx = 0 \quad 0 < b < a$$

$$= \infty \quad b = a$$

$$= \frac{-1}{\sqrt{b^2 - a^2}} \quad a < b < \infty$$

Using the above formulae, we can write

$$E_1(P) = \frac{\beta}{\pi} \frac{1}{\sqrt{1 - \cos^2 \varphi}} = \frac{\beta}{\pi} \frac{1}{\sin \varphi} = \frac{-j\pi(\epsilon_r - 1) \bar{t}}{\sin \varphi}$$

which is the required expression for the scattered field due to an infinite dielectric sheet.

Calculation of $E_2(P)$

Setting $\beta = -j\pi^2(\epsilon_r - 1) \bar{t}$, we have

$$E_2(P) = \beta \left\{ \int_{-\infty}^{-\bar{l}} H_0^{(2)}(2\pi|\bar{x}|) e^{j2\pi\bar{x} \cos \varphi} d\bar{x} + \int_{\bar{l}}^{\infty} H_0^{(2)}(2\pi|\bar{x}|) e^{j2\pi\bar{x} \cos \varphi} d\bar{x} \right\}$$

$$= \beta \left\{ \int_{\bar{l}}^{\infty} H_0^{(2)}(2\pi\bar{x}) e^{-j2\pi\bar{x} \cos \varphi} d\bar{x} + \int_{\bar{l}}^{\infty} H_0^{(2)}(2\pi\bar{x}) e^{j2\pi\bar{x} \cos \varphi} d\bar{x} \right\}$$

If \bar{l} is about one-half or greater (as in the experiments performed), the Hankel function can be very closely approximated by the following formula:

$$H_0^{(2)}(2\pi\bar{x}) \doteq \frac{1}{\pi\sqrt{\bar{x}}} e^{-j(2\pi\bar{x} - \frac{\pi}{4})}$$

Making this substitution, we have

$$\begin{aligned} E_2(P) &= \frac{\beta}{\pi} e^{j\frac{\pi}{4}} \left\{ \int_{\bar{l}}^{\infty} \frac{e^{-j2\pi\bar{x}(1+\cos\varphi)}}{\sqrt{\bar{x}}} d\bar{x} + \int_{\bar{l}}^{\infty} \frac{e^{-j2\pi\bar{x}(1-\cos\varphi)}}{\sqrt{\bar{x}}} d\bar{x} \right\} \\ &= \frac{\beta}{\pi} e^{j\frac{\pi}{4}} \left\{ \int_{\bar{l}}^{\infty} \frac{e^{-j\gamma_1\bar{x}}}{\sqrt{\bar{x}}} d\bar{x} + \int_{\bar{l}}^{\infty} \frac{e^{-j\gamma_2\bar{x}}}{\sqrt{\bar{x}}} d\bar{x} \right\} \end{aligned}$$

where $\gamma_1 = 2\pi(1 + \cos\varphi)$ and $\gamma_2 = 2\pi(1 - \cos\varphi)$.

It is now necessary to evaluate integrals of the form

$$\int_a^{\infty} \frac{e^{-j\gamma x}}{\sqrt{x}} dx = \int_a^{\infty} \frac{\cos \gamma x}{\sqrt{x}} dx - j \int_a^{\infty} \frac{\sin \gamma x}{\sqrt{x}} dx$$

These will be expressed in terms of the Fresnel integrals C and S which are defined as follows (see reference 7):

$$C\left(\sqrt{\frac{2v}{\pi}}\right) = \frac{1}{\sqrt{2\pi}} \int_0^v \frac{\cos u}{\sqrt{u}} du, \quad S\left(\sqrt{\frac{2v}{\pi}}\right) = \frac{1}{\sqrt{2\pi}} \int_0^v \frac{\sin u}{\sqrt{u}} du.$$

Since $S(\infty) = C(\infty) = \frac{1}{2}$, it is possible to change the range of integration to obtain

$$\int_v^{\infty} \frac{\cos u}{\sqrt{u}} du = \sqrt{2\pi} \left[\frac{1}{2} - C \left(\sqrt{\frac{2v}{\pi}} \right) \right]$$

$$\int_v^{\infty} \frac{\sin u}{\sqrt{u}} du = \sqrt{2\pi} \left[\frac{1}{2} - S \left(\sqrt{\frac{2v}{\pi}} \right) \right]$$

Returning to the integral form found in the problem, we make the transformation $\gamma x = u$ which gives

$$\begin{aligned} \int_a^{\infty} \frac{e^{-j\gamma x}}{\sqrt{x}} dx &= \frac{1}{\sqrt{\gamma}} \int_{\gamma a}^{\infty} \frac{e^{-ju}}{\sqrt{u}} du = \frac{1}{\sqrt{\gamma}} \int_{\gamma a}^{\infty} \frac{\cos u}{\sqrt{u}} du - j \frac{1}{\sqrt{\gamma}} \int_{\gamma a}^{\infty} \frac{\sin u}{\sqrt{u}} du \\ &= \sqrt{\frac{2\pi}{\gamma}} \left[\frac{1}{2} - C \left(\sqrt{\frac{2\gamma a}{\pi}} \right) \right] - j \sqrt{\frac{2\pi}{\gamma}} \left[\frac{1}{2} - S \left(\sqrt{\frac{2\gamma a}{\pi}} \right) \right] = \sqrt{\frac{2\pi}{\gamma}} \left[F_c(\gamma a) - j F_s(\gamma a) \right] \end{aligned}$$

where

$$F_c(\gamma a) = \frac{1}{2} - C \left(\sqrt{\frac{2\gamma a}{\pi}} \right)$$

$$F_s(\gamma a) = \frac{1}{2} - S \left(\sqrt{\frac{2\gamma a}{\pi}} \right)$$

The functions C and S are tabulated in reference 7 for γa from 0 to 50 in .01 steps.

It is now possible to obtain the field $E_2(P)$ in terms of the tabulated functions.

$$\begin{aligned}
 E_2(P) &= \frac{\beta}{\pi} e^{j\frac{\pi}{4}} \left\{ \sqrt{\frac{2\pi}{\gamma_1}} \left[F_c(\gamma_1 \bar{l}) - j F_s(\gamma_1 \bar{l}) \right] + \sqrt{\frac{2\pi}{\gamma_2}} \left[F_c(\gamma_2 \bar{l}) - j F_s(\gamma_2 \bar{l}) \right] \right\} \\
 &= \frac{\beta}{\pi} e^{j\frac{\pi}{4}} \left\{ \frac{F_c(\gamma_1 \bar{l}) - j F_s(\gamma_1 \bar{l})}{\sqrt{1 + \cos \varphi}} + \frac{F_c(\gamma_2 \bar{l}) - j F_s(\gamma_2 \bar{l})}{\sqrt{1 - \cos \varphi}} \right\} \\
 &= \frac{\beta e^{j\frac{\pi}{4}}}{\pi \sin \varphi} \left\{ \sqrt{1 - \cos \varphi} \left[F_c(\gamma_1 \bar{l}) - j F_s(\gamma_1 \bar{l}) \right] + \sqrt{1 + \cos \varphi} \left[F_c(\gamma_2 \bar{l}) - j F_s(\gamma_2 \bar{l}) \right] \right\}
 \end{aligned}$$

Now $\sqrt{1 + \cos \varphi} = \sqrt{2} \cos \frac{\varphi}{2}$ and $\sqrt{1 - \cos \varphi} = \sqrt{2} \sin \frac{\varphi}{2}$ and in addition $e^{j\frac{\pi}{4}} = \frac{1+j}{\sqrt{2}}$. Thus we have

$$\begin{aligned}
 E_2(P) &= \frac{\beta(1+j)}{\pi \sin \varphi} \left\{ \sin \frac{\varphi}{2} \left[F_c(\gamma_1 \bar{l}) - j F_s(\gamma_1 \bar{l}) \right] + \cos \frac{\varphi}{2} \left[F_c(\gamma_2 \bar{l}) - j F_s(\gamma_2 \bar{l}) \right] \right\} \\
 &= \frac{\beta(1+j)}{\pi \sin \varphi} \left\{ \sin \frac{\varphi}{2} F_c(\gamma_1 \bar{l}) + \cos \frac{\varphi}{2} F_c(\gamma_2 \bar{l}) \right. \\
 &\quad \left. - j \left[\sin \frac{\varphi}{2} F_s(\gamma_1 \bar{l}) + \cos \frac{\varphi}{2} F_s(\gamma_2 \bar{l}) \right] \right\} \\
 &= \frac{\beta}{\pi \sin \varphi} \left\{ \sin \frac{\varphi}{2} \left[F_c(\gamma_1 \bar{l}) + F_s(\gamma_1 \bar{l}) \right] + \cos \frac{\varphi}{2} \left[F_c(\gamma_2 \bar{l}) + F_s(\gamma_2 \bar{l}) \right] \right. \\
 &\quad \left. + j \sin \frac{\varphi}{2} \left[F_c(\gamma_1 \bar{l}) - F_s(\gamma_1 \bar{l}) \right] + j \cos \frac{\varphi}{2} \left[F_c(\gamma_2 \bar{l}) - F_s(\gamma_2 \bar{l}) \right] \right\} \\
 &= \frac{\beta}{\pi \sin \varphi} \{ N + jM \} = \frac{-j\pi(\epsilon_r - 1)t}{\sin \varphi} \{ N + jM \}
 \end{aligned}$$

where

$$N = \sin \frac{\varphi}{2} \left[F_c(\gamma_1 \bar{\ell}) + F_s(\gamma_1 \bar{\ell}) \right] + \cos \frac{\varphi}{2} \left[F_c(\gamma_2 \bar{\ell}) + F_s(\gamma_2 \bar{\ell}) \right]$$

$$= \sin \frac{\varphi}{2} \left[1 - S \left(\sqrt{\frac{2\gamma_1 \bar{\ell}}{\pi}} \right) - C \left(\sqrt{\frac{2\gamma_1 \bar{\ell}}{\pi}} \right) \right] + \cos \frac{\varphi}{2} \left[1 - S \left(\sqrt{\frac{2\gamma_2 \bar{\ell}}{\pi}} \right) - C \left(\sqrt{\frac{2\gamma_2 \bar{\ell}}{\pi}} \right) \right]$$

$$M = \sin \frac{\varphi}{2} \left[F_c(\gamma_1 \bar{\ell}) - F_s(\gamma_1 \bar{\ell}) \right] + \cos \frac{\varphi}{2} \left[F_c(\gamma_2 \bar{\ell}) - F_s(\gamma_2 \bar{\ell}) \right]$$

$$= \sin \frac{\varphi}{2} \left[S \left(\sqrt{\frac{2\gamma_1 \bar{\ell}}{\pi}} \right) - C \left(\sqrt{\frac{2\gamma_1 \bar{\ell}}{\pi}} \right) \right] + \cos \frac{\varphi}{2} \left[S \left(\sqrt{\frac{2\gamma_2 \bar{\ell}}{\pi}} \right) - C \left(\sqrt{\frac{2\gamma_2 \bar{\ell}}{\pi}} \right) \right]$$

$$\gamma_1 = 2\pi(1 + \cos \varphi)$$

$$\gamma_2 = 2\pi(1 - \cos \varphi)$$

Thus, with the help of a table of Fresnel integrals S and C, the values of M and N can be calculated for any given $\bar{\ell}$ and φ .

The Total Field E(P)

E(P) is given by the relation

$$E(P) = 1 + E_1(P) - E_2(P) = 1 + \frac{\beta}{\pi} \cdot \frac{1}{\sin \varphi} - \frac{\beta}{\pi} \cdot \frac{1}{\sin \varphi} [N + jM]$$

$$= 1 + \frac{\beta}{\pi \sin \varphi} [1 - N - jM] = 1 - \frac{\pi(\epsilon_r - 1)\bar{t}}{\sin \varphi} [M + j(1 - N)]$$

The radiation pattern $P(\varphi)$ is given by the absolute value of E(P).

APPENDIX D

The Asymptotic Form of the Fresnel Integral Solution

One form of the Fresnel integral can be expressed asymptotically as follows:

$$\sqrt{\frac{2}{\pi}} \int_b^{\infty} e^{-jt^2} dt \sim \frac{e^{-jb^2}}{jb \sqrt{2\pi}} \left[1 - \frac{j}{2b^2} + \dots \right] \sim \frac{e^{-jb^2}}{jb \sqrt{2\pi}}$$

if $2b^2 \gg 1$

Making the transformation $t^2 = \gamma x$ and $b^2 = \gamma a$, we obtain

$$\int_a^{\infty} \frac{e^{-j\gamma x}}{\sqrt{x}} dx \sim \frac{e^{-j\gamma a}}{j\gamma \sqrt{a}}$$

if $2\gamma a \gg 1$

From Appendix C we have an expression for $E_2(P)$, the scattered field at the origin when a plane wave is incident on two co-planar semi-infinite dielectric sheets.

$$E_2(P) = \frac{\beta}{\pi} e^{j\frac{\pi}{4}} \left\{ \int_{\bar{l}}^{\infty} \frac{e^{-j\gamma_1 \bar{x}}}{\sqrt{\bar{x}}} d\bar{x} + \int_{\bar{l}}^{\infty} \frac{e^{-j\gamma_2 \bar{x}}}{\sqrt{\bar{x}}} d\bar{x} \right\}$$

where $\gamma_1 = 2\pi(1 + \cos \varphi)$, $\gamma_2 = 2\pi(1 - \cos \varphi)$. If $2\gamma_1 \bar{l} \gg 1$ and $2\gamma_2 \bar{l} \gg 1$ we can write

$$\begin{aligned}
 E_2(P) &= \frac{\beta}{\pi} e^{j\frac{\pi}{4}} \left\{ \frac{e^{-j\gamma_1 \bar{l}}}{j\gamma_1 \sqrt{\bar{l}}} + \frac{e^{-j\gamma_2 \bar{l}}}{j\gamma_2 \sqrt{\bar{l}}} \right\} \\
 &= - \frac{\pi(\epsilon_r - 1)\bar{t}}{2} \frac{e^{j\frac{\pi}{4}}}{\pi \sqrt{\bar{l}}} \left\{ \frac{e^{-j2\pi\bar{l}(1+\cos\varphi)}}{1 + \cos\varphi} + \frac{e^{-j2\pi\bar{l}(1-\cos\varphi)}}{1 - \cos\varphi} \right\} \\
 &= - \frac{\pi(\epsilon_r - 1)\bar{t}}{2} \frac{e^{-j(2\pi\bar{l} - \frac{\pi}{4})}}{\pi \sqrt{\bar{l}}} \left\{ \frac{e^{-j2\pi\bar{l} \cos\varphi}}{1 + \cos\varphi} + \frac{e^{+j2\pi\bar{l} \cos\varphi}}{1 - \cos\varphi} \right\}
 \end{aligned}$$

Now the large-argument approximation to the Hankel function $H_0^{(2)}(2\pi\bar{l})$ is given by

$$H_0^{(2)}(2\pi\bar{l}) \doteq \frac{e^{-j(2\pi\bar{l} - \frac{\pi}{4})}}{\pi \sqrt{\bar{l}}} = R(\bar{l})$$

Thus we can write

$$E_2(P) = - \frac{\pi(\epsilon_r - 1)\bar{t}}{2} R(\bar{l}) \left[\frac{e^{-j2\pi\bar{l} \cos\varphi}}{1 + \cos\varphi} + \frac{e^{+j2\pi\bar{l} \cos\varphi}}{1 - \cos\varphi} \right]$$

It has already been shown in Appendix A that $E_1(P)$ is given by

$$E_1(P) = -j \frac{\pi(\epsilon_r - 1)\bar{t}}{\sin\varphi}$$

The total field at the origin $E(P)$ now can be obtained using the asymptotic formulae. We have

$$E(P) = 1 + E_1(P) - E_2(P)$$

$$= 1 + \pi(\epsilon_r - 1) \bar{t} \left\{ \frac{-j}{\sin \varphi} + \frac{R(\bar{l})}{2} \left[\frac{e^{-j2\pi\bar{l} \cos \varphi}}{1 + \cos \varphi} + \frac{e^{+j2\pi\bar{l} \cos \varphi}}{1 - \cos \varphi} \right] \right\}$$

This formula has been derived using the asymptotic expansion for the

Fresnel integral and holds if $2\gamma_1 \bar{l} \gg 1$ and $2\gamma_2 \bar{l} \gg 1$. That is

$4\pi\bar{l}(1 \pm \cos \varphi) \gg 1$ which means that, for a fixed value of \bar{l} , φ is not permitted to approach 0° or 180° .

In the above formula the factor $(j \sin \varphi)^{-1}$ comes from an integration over an infinite dielectric sheet. The other term

$$\frac{R(\bar{l})}{2} \left[\frac{e^{-j2\pi\bar{l} \cos \varphi}}{1 + \cos \varphi} + \frac{e^{+j2\pi\bar{l} \cos \varphi}}{1 - \cos \varphi} \right]$$

suggests that the thin dielectric strip may be represented by two infinite line sources in free space. These equivalent line sources are located at $x = -\bar{l}$ and $x = +\bar{l}$. Furthermore these equivalent line sources have individual radiation patterns of the form $(1 \pm \cos \varphi)^{-1}$.

Now $E(P)$ is of the form $E(P) = 1 + (\epsilon_r - 1) \bar{t} G$ where G is a complex number and a function of φ and \bar{l} . If $(\epsilon_r - 1) \bar{t}$ is very small so that the magnitude of $(\epsilon_r - 1) \bar{t} G$ is much smaller than one, then the radiation pattern given by $P(\varphi) = |1 + (\epsilon_r - 1) \bar{t} G|$ can be approximated by $P(\varphi) = 1 + R_e \left\{ (\epsilon_r - 1) \bar{t} G \right\}$ where R_e indicates "the real part of". Thus the radiation pattern formula becomes

$$P(\varphi) = 1 + \pi(\epsilon_r - 1) \bar{t} R_e \left\{ \frac{R(\bar{l})}{2} \left[\frac{e^{-j2\pi\bar{l} \cos \varphi}}{1 + \cos \varphi} + \frac{e^{+j2\pi\bar{l} \cos \varphi}}{1 - \cos \varphi} \right] \right\}$$

The expression inside the curly brackets is the line source term described in the previous paragraph. Thus a thin dielectric strip with a low dielectric constant can be represented approximately by two line sources in free space.

The "Two-Source Equivalent" with Directivity

This report deals with values of ℓ which are integral multiples of a half wavelength. Thus we may set $\bar{\ell} = \frac{n}{2}$ where n is an integer. The above formula for $P(\varphi)$ can be simplified and written as

$$P(\varphi) = 1 + \frac{(\epsilon_r - 1) \bar{t} (-1)^n}{\sqrt{n}} \left[\frac{\cos(n\pi \cos \varphi) - \cos \varphi \sin(n\pi \cos \varphi)}{\sin^2 \varphi} \right]$$

where the directivity factors $(1 \pm \cos \varphi)^{-1}$ have been included.

The "Two-Source Equivalent" without Directivity

If φ is further restricted to be not far from 90° , then we may make the approximations $\sin \varphi \doteq 1$ and $\cos \varphi \doteq 0$. This means that the directivity factors $(1 \pm \cos \varphi)^{-1}$ become unity and the dielectric strip is represented by two ordinary non-directive line sources. The radiation pattern formula becomes

$$P(\varphi) = 1 + (\epsilon_r - 1) \bar{t} \frac{(-1)^n}{\sqrt{n}} \cos(n\pi \cos \varphi)$$

where, as before, n is an integer and gives the number of half-wavelengths in the length ℓ .

APPENDIX E

When an electromagnetic wave propagates along a dielectric slab, the wavelength is shorter than in free space. The ratio of guided wavelength λ_g to free space wavelength λ can be obtained by the source-free solutions of Maxwell's equations for an infinite dielectric slab in space. Such solutions result in the following characteristic equations for the TE modes:

$$\tan \left[\frac{k_x t}{2} \right] = \sqrt{\frac{k_1^2 - k_0^2}{k_x^2} - 1}$$

$$- \cot \left[\frac{k_x t}{2} \right] = \sqrt{\frac{k_1^2 - k_0^2}{k_x^2} - 1}$$

The propagation constant along the dielectric slab is given by

$$k_l = \sqrt{k_1^2 - k_x^2}$$

and the wavelength ratio is

$$\frac{\lambda_g}{\lambda} = \frac{k_0}{k_l}$$

where

t = dielectric slab thickness

$k_0 = \omega \sqrt{\mu_0 \epsilon_0} = \frac{2\pi}{\lambda}$ = the propagation constant in free space

$k_1 = \omega \sqrt{\mu_0 \epsilon_0 \epsilon_r}$ = the propagation constant in a dielectric medium of relative dielectric constant ϵ_r .

$k_{\ell} = \frac{2\pi}{\lambda_g}$ = longitudinal propagation constant for a dielectric slab in space.

For very thin dielectric slabs, only the lowest order TE mode can propagate and this mode has no cutoff frequency. For the lowest order TE mode, the propagation constant k_{ℓ} (and consequently the ratio $\frac{\lambda_g}{\lambda}$) can be obtained from the solution of the transcendental equation

$$\tan \left[\frac{k_x t}{2} \right] = \sqrt{\frac{k_1^2 - k_o^2}{k_x^2} - 1}$$

For the case of a polystyrene slab ($\epsilon_r = 2.55$), the values of $\frac{\lambda_g}{\lambda}$ are tabulated below.

$\frac{t}{\lambda}$	t (in inches at 5000 mc)	$\frac{\lambda_g}{\lambda}$
.1058	1/4 "	.908
.05292	1/8 "	.972
.02646	1/16"	.994
.01323	1/32"	.998

If t is assumed to be very small, the above transcendental equation can be put into a very simple form. The use of a trigonometric fundamental identity changes the equation to

$$\cos^2 \frac{k_x t}{2} = \frac{k_x^2}{k_1^2 - k_o^2}$$

The half-angle formula gives

$$\cos k_x t = \frac{2k_x^2}{k_1^2 - k_o^2} - 1$$

The assumption that t is small permits the approximation

$$\cos k_x t \doteq 1 - \frac{k_x^2 t^2}{2}$$

which puts the equation into the form

$$k_x^2 = \left(\frac{1}{k_1^2 - k_o^2} + \frac{t^2}{4} \right)^{-1}$$

Now $k_x^2 = k_1^2 - k_\ell^2$ and $k_1^2 - k_o^2 = k_o^2(\epsilon_r - 1)$. Making these substitutions and appropriate binomial approximations (assuming t to be small)

we get the approximate expression for k_ℓ ,

$$k_\ell = k_o \left[1 + \frac{\pi^2}{2} \left\{ (\epsilon_r - 1) \frac{t}{\lambda} \right\}^2 \right]$$

from which the desired values of $\frac{\lambda_g}{\lambda}$ can be calculated. These are given in the following table and compared with the results of the direct computation of the transcendental equation solution. ($\epsilon_r = 2.55$).

$\frac{t}{\lambda}$	$\frac{\lambda_g}{\lambda}$	
	Exact	Approximate
.1058	.908	.868
.05292	.972	.967
.02646	.994	.992
.01323	.998	.998

There are two interesting similarities between the above approximate formula and the radiation pattern formula (iteration series solution). Both formulae are accurate over the same range of ϵ_r and t , and the factor $(\epsilon_r - 1) \frac{t}{\lambda}$ is prominent in both expressions.

